



Research papers

Multiobjective stochastic programming with recourses for real-time flood water conservation of a multireservoir system under uncertain forecasts

Bin Xu*, Ping-an Zhong*, Qingwen Lu, Feilin Zhu, Xin Huang, Yufei Ma, Jisi Fu

College of Hydrology and Water Resources, Hohai University, NO. 1, Xikang Road, Nanjing 210098, China

ARTICLE INFO

This manuscript was handled by Marco Borga, Editor-in-Chief, with the assistance of Baptiste François, Associate Editor

Keywords:

Reservoir operation
Flood water conservation
Forecast uncertainty
Stochastic programming with recourses
Multiobjective optimization

ABSTRACT

Flood water conservation realized through real-time multireservoir operations is effective in mitigating water scarcity. Owing to the influence of real-time inflow forecast uncertainty, determining an informed operation plan necessitates resolution of the conflict between upstream flood risk, downstream flood risk, and water scarcity risk. This study developed a multiobjective stochastic programming with recourses (MOSP) model to seek robust risk-averse plans under multiple risks. In the proposed approach, inflow forecast errors are modeled and sampled as spatially and temporally correlated stochastic processes using a copula function. The multiobjective stochastic programming is solved using the epsilon constraint method based on explicit formulation of multiple risk objectives with discretized inflow scenarios, and a rolling horizon with recourses for real-time operational updating is modeled to address the dynamic decision-making characteristics. The proposed methodologies were applied to the multireservoir system of the Pi River Basin (China), and comparisons with model results of a traditional coupled simulation and a deterministic single objective optimization model were conducted. Results indicated that capturing spatial and temporal dependencies of forecast uncertainty provides informative forecast support. Moreover, noninferior solutions obtained from MOSP dominate the deterministic optimal solution, which could either conserve 4.86 million m³ (12%) more water without increase in flood risk, or reduce the upstream flood risk by 3.1% without increase in either water scarcity or downstream flood risk during a typical receding flood. The proposed methodology provides a dynamic decision-making modeling tool that could reduce overall risk and determine a compromise for flood water conservation under uncertainty.

1. Introduction

Water scarcity problem affects sustainable socioeconomic development and threatens ecological safety (Chen et al., 2016a, 2016b; Wen et al., 2018). Being listed in 2019 by the World Economic Forum as one of the greatest global risks of the next decade, this problem is expected to have intensified influence owing to increasing water demand and the changing climate (Cai et al., 2018a, 2018b; Zhang et al., 2018; Piao et al., 2010; Shi et al., 2018; Sahukhal and Bajracharya, 2019). Reservoir operations (Yeh, 1985; Labadie, 2004) that redistribute variable inflow processes according to water demand variations represent important measures for securing the water supply. Partial conservation of flood water during receding flood events and delivery of conserved water (flood resource utilization) before the occurrence of the next flood, managed through reservoir operations, is one possible approach that could alleviate the problem of water scarcity and its secondary hazardous influences (Li et al., 2010; Mao et al., 2019). This approach,

which has received widespread research attention, has been put into operational practice in China (Liu et al., 2015; Ouyang et al., 2015). The key technique to informed flood water conservation through reservoir operations is real-time adaptive control of the flood limited water level (FLWL) to determine a tradeoff between flood control and water supply, such that the associated flood risk is both manageable and acceptable (Ding et al., 2015; Xu et al., 2020).

According to the Chinese Flood Control Act, before the occurrence of a flood, the reservoir water level should be maintained below the FLWL such that the reservoir system preserves adequate flood storage for regulating design floods (Yun and Singh, 2008). However, this policy results in frequent spillage because it limits the storage capacity of a reservoir to regulate small floods. To ensure conservation of flood water without violating the requirement of the design flood standard, previous related studies have introduced the concept of real-time dynamic control of the FLWL (DCFLWL) (Li et al., 2010). The idea behind DCFLWL is to control the water level to below a certain bound, which is

* Corresponding authors.

E-mail addresses: xubin_hhu@hhu.edu.cn (B. Xu), pazhong@hhu.edu.cn (P.-a. Zhong), luqw@hhu.edu.cn (Q. Lu), zhufeilin@hhu.edu.cn (F. Zhu), xinhuang@hhu.edu.cn (X. Huang), mayufei@hhu.edu.cn (Y. Ma).

determined according to the prerelease capacity, within an effective forecast lead time. Thus, the water level can be safely drawn down to the designed FLWL even if a flood is anticipated. In an interconnected reservoir system, flood conservation can further explore the synergistic effects of joint reservoir operations, which can either increase the conservation level or decrease the flood risk when compared with the individual operations (Zhou et al., 2018). For a multireservoir system, joint operation that seeks complementarity among the reservoir storages through hydraulic connections has been proposed (Zhou et al., et al., 2014; Ouyang et al., 2015). This approach allows some reservoirs within the system to conserve flood water by raising their FLWLs if the current water level of certain other reservoirs are below their FLWLs. By extending the capacity-constrained prerelease model from a single reservoir to a multireservoir system (Chen et al., 2013). Zhou et al., (2014) introduced the aggregation and disaggregation method for synthesizing a reservoir system into an aggregated reservoir. This permits determination of both the total upper bound of the FLWLs of the entire system and the dispatch of the total bound to each single reservoir on the premise of maintaining the same flood control standard. Zhong et al., (2014) proposed a DCFLWL model for a dual-reservoir cascade system for determining the storage complementarity relationship. In their study, the upper bound of the FLWL of one reservoir was determined based on the vacant flood storage of the other reservoir.

Previous studies have identified that DCFLWL through real-time reservoir operations is influenced by multiple uncertainties (Huang et al., 2018), among which forecast uncertainty has been determined as the primary source, resulting in flood risk when the forecast inflow underestimates the actual inflow. This is caused by the inability of a forecast to capture precise inflow information (Zhang et al., 2019; Cloke and Pappenberger, 2009), especially for periods beyond the effective forecast lead time. For reducing water scarcity risk, informed flood water conservation should not increase flood risk. Therefore, this necessitates both risk analysis to evaluate the flood risk associated with the conservation level (i.e., surplus water conserved above the storage of the designed FLWL) and risk decision making to determine a suitable strategy under an acceptable risk level. Early efforts in flood water conservation modeling separated risk analysis and risk decision making into two phases using a sensitivity analysis framework: (1) obtaining finite conservation plans with varied flood risk levels; and (2) selecting the most suitable one through screening analysis. Li et al., (2010) considered the inflow forecast error and the uncertainty of a flood hydrograph shape as sources of uncertainty, and they established a Monte Carlo simulation model to determine the variation range of FLWL without increasing flood risk. Tan et al., (2017) developed a storage-complementing regulation model to derive the FLWLs of a cascade reservoir system using a copula function to address the dependency of the spatial pattern of the flood. Actually, a coupled simulation and sensitivity analysis method implicitly treats flood risk as a soft constraint when determining a conservation plan. This represents a modeling tool for presenting the surrogate tradeoff between conservation benefit and flood risk, but it does not aim to reduce or control the risk directly. Consequently, the selected plan could be suboptimal in terms of either benefit maximization or risk minimization. Alternative modeling techniques introduced the stochastic optimization method to address stochasticity, and then optimized the net utility through joint consideration of the conservation benefit and the loss of flood risk. Ding et al., (2015) analytically derived a two-stage risk-hedging rule to minimize the weighted sum of water scarcity risk and flood risk through hedging. Although these studies provided remarkable support for determining and interpreting optimal operation plan, lacking of elaborating the dynamic decision making modeling under correlated uncertainties could limit the overall robustness or optimality of plans, especially for application in complex reservoirs system. Specifically, limitations of previous studies include: 1) weakening the consideration of spatial and temporal correlations of forecasting errors involved in the reservoirs system, which could result in biases in risk evaluation (Chen

et al., 2016a, 2016b); 2) failing to directly optimize the flood risks of upstream reservoirs, downstream protection regions and water scarcity risk within a multi-objective context, potentially yields dominated solutions that are inferior in maintaining robustness and reliability in multiple risks (Watkins and McKinney, 1997); and 3) lacking the explicit modeling with rolling horizon and recourse decisions for mitigating the negative consequence of forecasting error and conservation decisions based on uncertain and partial forecasts in a limited forecast horizon (Zhao et al., 2012).

Informed decision making for determining the conservation and release strategies of a complex reservoir system, based on partial and uncertain forecasts, represents a multistage, multiobjective, and risky decision-making problem (Pan et al., 2015; Xu et al., 2015). Recognizing the inability to adapt the influence of uncertainties and risks through operation in deterministic optimization, stochastic programming with recourses (Xu et al., 2019; King and Wallace, 2012; Housh et al., 2013) provides opportunities to hedge or control the risks via constraining current stage decisions with uncertainties preprocessed as discretized scenarios. In finding a solution that satisfies the constraints for all (or almost all) possible estimated scenarios, and in targeting optimization of risk or benefit objectives (Etkin et al., 2015; Xu et al., 2017), both the robustness and the optimality of decisions under uncertainties can be ensured. Compared with stochastic dynamic programming (Turgeon, 2007; Haguma et al., 2018; Piantadosi et al., 2008), stochastic programming is flexible in using synthetic scenarios or ensemble forecasts (Nayak et al., 2018; Cloke and Pappenberger, 2009) preserving multistage serial correlations, which can capture abundant characteristics of the uncertainties. Conventional stochastic programming models generally tackle the problem of single objective optimization without consideration of the resolution of conflict amongst competing risk objectives. As water scarcity risk and flood risk in relation to flood water conservation are conflicting and incommensurable, resolving the conflict involves multiobjective decision making, which generates candidate noninferior solution sets through vector (Emmerich and Deutz, 2018; Tsoukalas and Makropoulos, 2015) or scalar optimizations (Huang et al., 2019). It eventually allows selection of a compromise solution from the generated sets based on tradeoffs (Tang et al., 2019) and the preferences of decision makers (Kodikara et al., 2010).

The desire to bridge the three knowledge gaps mentioned above motivated the current study. Distinct from previous related work, the objectives of this study were as follows: 1) to generate uncertain inflow scenarios with preserved spatial and temporal correlations using copula functions (Peng et al., 2017; Chen et al., 2016a, 2016b, 2020) for refining uncertainty characterization; 2) to develop and solve a multi-objective stochastic programming with recourses (MOSP) model for providing noninferior flood water conservation strategies for a multireservoir system; and 3) to inform decision making by selecting a risk-robust noninferior strategy and analyzing the advantages of the solution through comparative experiments with deterministic optimization solution.

2. Methodology

Fig. 1 depicts a flowchart illustrating a coupled model framework for informing flood water conservation of a multireservoir system under uncertainty, which generally includes three subsections. First, the real-time inflow forecast uncertainty simulated with temporal and spatial dependencies captured using a copula function model is discussed in **Section 2.1**. Thereafter, based on generated inflow scenarios, the traditional deterministic optimization model using aggregation and decomposition of systems for generating the benchmark solution under each scenario is reviewed in **Section 2.2**. Finally, the proposed MOSP is established with coupled multiobjective optimization and stochastic programming in **Section 2.3**.

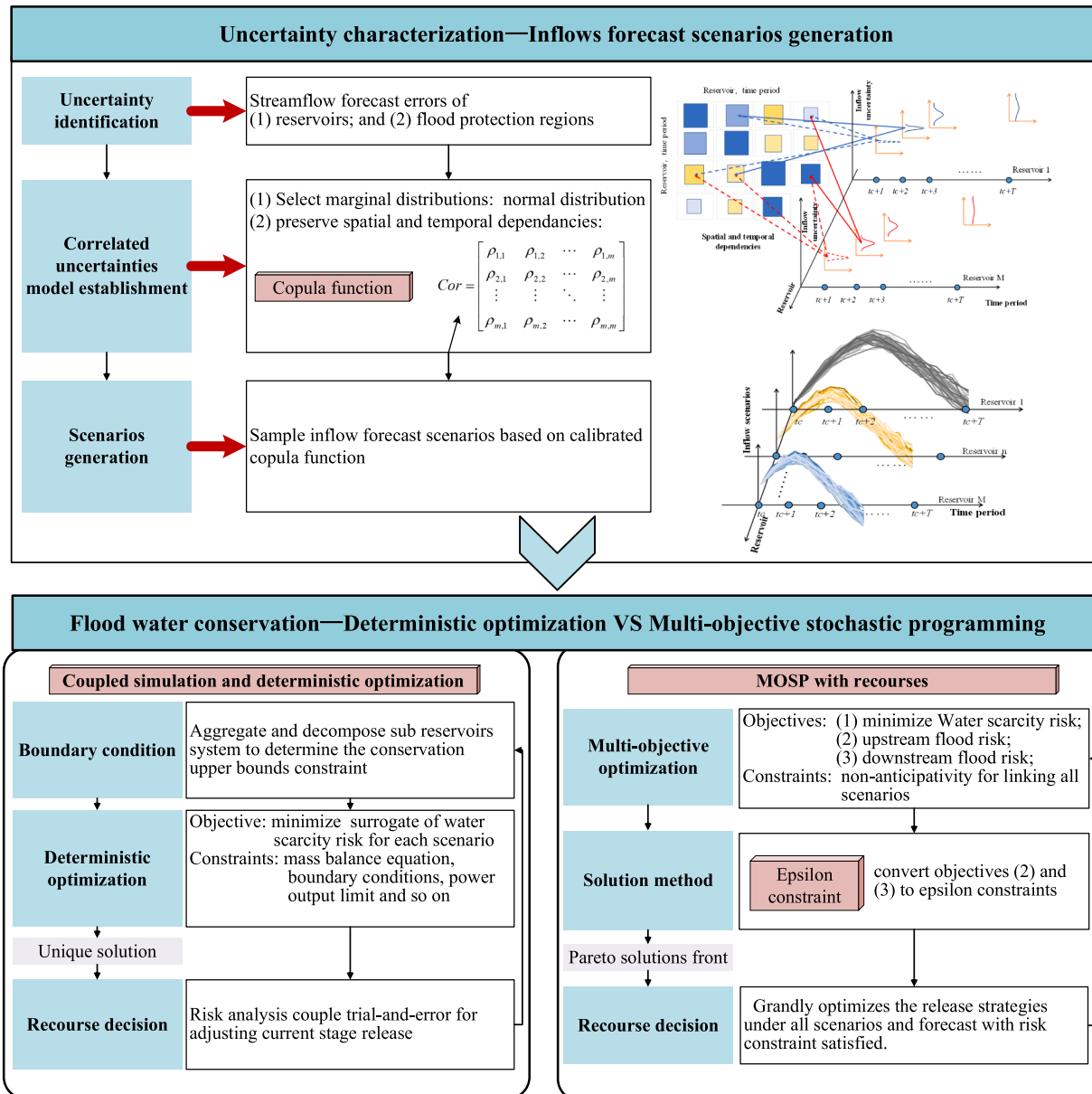


Fig. 1. Flow chart of process for coupling the MOSP model framework for real-time flood water conservation of a multireservoir system under uncertain forecasts.

2.1. Inflows forecast uncertainty characterization using a copula function

Conserving flood water through reservoir operation via dynamic variation of the FLWL requires the support of natural real-time inflow forecasts, which are generated by a hydrological forecast model driven by the inputs of observed and forecasted precipitation sequences. The errors in inflow forecasts, which stem from input errors, model parameter errors, and model structure errors (Si et al., 2019), result in forecast uncertainty. Often, owing to the persistent influence of errors throughout the forecast model chain, forecast uncertainty can be correlated spatially and temporally. Characterization of the correlated uncertainties provides refined input for reservoir operation modeling for both risk analysis and decision making.

2.1.1. Forecast uncertainty identification

We can consider a general multireservoir system with the operational objectives of providing flood control and water supply, protecting the safety of M reservoirs and $N + 1$ downstream protection regions, and supplying water to the furthermost downstream cities and

irrigation areas. Then, we suppose the system could be decomposed into N subsystems in terms of the topology (i.e., single reservoir systems, cascade reservoir systems, and parallel reservoir systems with the total numbers of G , J , and K , respectively, $G + J + K = N$), and that each system protects one direct (private) downstream protection region, whereas the entire system jointly protects the furthermost downstream (public) protection region. A schematic of such a multireservoir system and the decomposition is shown in Fig. 2.

Forecast uncertainty arises when the actual streamflow is biased with the forecast. It means that the safety of flood control might be threatened when the actual streamflow is underestimated because surplus flood water causes unexpected increase in either reservoir storage or river channel water level. Considering the complex hydraulic continuity relation within a complex reservoir system, joint operation should incorporate analysis of inflow and lateral inflow forecast errors. Accordingly, the source of uncertainty would be identified as follows:

$$\varepsilon_n(t) = (Iu_n^-(t) - Iu_n(t))/Iu_n^-(t), \quad n = 1, \dots, M; \quad t = tc + 1, \dots, tc + T \quad (1)$$

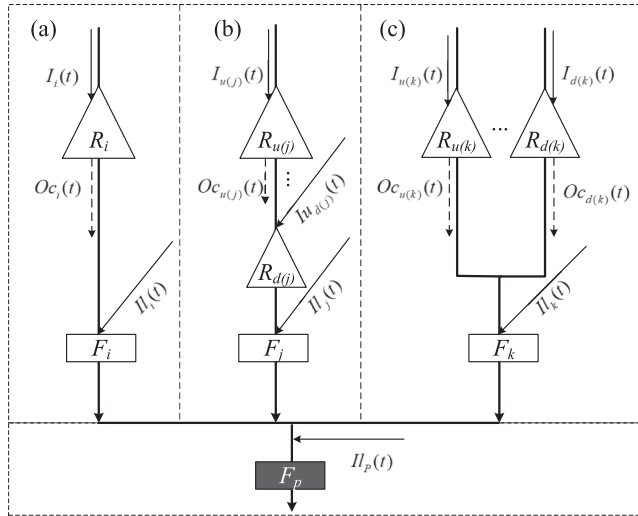


Fig. 2. Schematic of a multireservoir system for flood control and decomposition of a multireservoir subsystem: (a) single reservoir, (b) cascade reservoirs, and (c) parallel reservoirs.

$$\varepsilon f_{n'}(t) = (I_{l_n}(t) - I_{l_n'}(t)) / I_{l_n'}(t), \quad n' = 1, \dots, N+1; \quad t = tc + 1, \dots, tc + T \quad (2)$$

where $\varepsilon_n(t)$ and $\varepsilon f_{n'}(t)$ are the relative forecast errors (unit: %) in the lateral inflow of reservoir n and flood protection region n' , respectively, during time period t . Here, t is the index of time periods and tc is the current time period; the entire planning horizon comprises T time periods. The parameters $I_{l_n}(t)$ and $I_{l_n'}(t)$ are the corresponding actual lateral inflow (unit: m^3/s) of the reservoir and the flood protection region, respectively. If we assume a perfect forecast in the current time period, $\varepsilon_n(tc) = 0$ and $\varepsilon f_{n'}(tc) = 0$.

2.1.2. Characterization of correlated forecast errors using a copula function

Statistical based methods, which characterize forecast errors as stochastic processes and generate ensembles or scenario spread via Monte Carlo simulation, remain an appealing approach for risk analysis and sensitivity tests (Nester et al., 2012). Although many studies have noticed the temporal interdependencies of forecast error when modeling the dynamic evolution processes of streamflow forecasts for a single site (Chen et al., 2016a, 2016b; Zhao et al., 2013), most neglect the spatial interdependencies (Papaefthymiou and Pinson 2008). This study applied the copula function to model the joint distribution function of forecast errors and address their dependencies.

The copula function is a flexible tool for formulating a multivariate joint distribution by selecting arbitrary marginals and a dependence structure. According to Sklar's theorem (1959), the joint probability density function $f(x_1, x_2, \dots, x_m)$ of correlated random variables X_1, X_2, \dots, X_m can be determined by:

$$f(x_1, x_2, \dots, x_m) = c(u_1, u_2, \dots, u_m) \cdot f(x_1) \cdots f(x_m) \quad (3)$$

$$c(u_1, u_2, \dots, u_m) = \frac{\partial C(u_1, u_2, \dots, u_m)}{\partial u_1 \partial u_2 \dots \partial u_m} \quad (4)$$

$$F(x_i) = u_i, \quad i = 1, 2, \dots, m \quad (5)$$

where $f(x_1), \dots, f(x_m)$ and $F(x_1), \dots, F(x_m)$ are the marginal probability density functions and cumulative distribution functions of correlated variables X_1, X_2, \dots, X_m , respectively; $C(u_1, u_2, \dots, u_m)$ is the copula function.

Marginal distributions of forecast errors can be established and calibrated according to historical forecasted and observed samples of streamflow sequences, which are often considered to obey a normal distribution. Different dependence structures can be captured by various copula functions (copulas), i.e., the t copula, Gaussian copula,

Gumbel copula, Clayton copula, and Frank copula. The selection of a copula function and the calibration mainly use the dependence samples of forecast errors based on the maximum likelihood method and statistical tests.

Establishing the joint probability function of the forecast errors of a complex reservoir system falls into a rather high-dimensional case wherein data abundance and computational efforts trap modeling (Feng et al., 2019). To seek tractable approaches while maintaining as much information as possible, data preprocessing can be conducted to test the significance of the dependencies and reduce model size by neglecting insignificant dependencies information. For a rather highly complex system with remote and weak spatial connection among sub systems, spatial dependencies can also be neglected by treating forecast errors as spatial independent processes. Finally, the t copula is applied to model the joint probability density function of the forecast errors for its overall performance in information preservation and computation tractability, which is given by:

$$C(u, Cor, v)$$

$$= \int_{-\infty}^{t^{-1}(u_1)} \cdots \int_{-\infty}^{t^{-1}(u_m)} \frac{\Gamma\left(\frac{v+m}{v}\right)}{\Gamma\left(\frac{v}{2}\right)\sqrt{(\pi v)^m |Cor|}} \left(1 + \frac{1}{v} x^T Cor^{-1} x\right)^{\frac{v+m}{2}} dx, \quad (6)$$

where Cor is the correlation matrix, v denotes the degree of freedom; m equals $(M+N+1)T$ and variables X_1, X_2, \dots, X_m map to $\varepsilon_1(tc+1), \dots, \varepsilon_1(tc+T), \varepsilon_2(tc+1), \dots, \varepsilon_M(tc+T), \varepsilon f_1(tc+1), \dots, \varepsilon f_{N+1}(tc+T)$.

$$+ T)$$

Specifically, Cor can be calibrated by calculating the spatial and temporal correlation coefficient for each pair of forecast errors considered, as given by:

$$Cor = \begin{bmatrix} \rho_{1,1} & \rho_{1,2} & \cdots & \rho_{1,m} \\ \rho_{2,1} & \rho_{2,2} & \cdots & \rho_{2,m} \\ \vdots & \vdots & \ddots & \vdots \\ \rho_{m,1} & \rho_{m,2} & \cdots & \rho_{m,m} \end{bmatrix} \quad (7)$$

where $\rho_{i,j}$, $i, j = 1, 2, \dots, m$ is the linear correlation coefficient of variable X_i, X_j .

2.1.3. Scenarios generation for uncertain inflow forecasts

Discretized forecast streamflow scenarios of equal likelihood were generated using a Monte Carlo simulation that samples forecast errors using the calibrated copula function. This can be achieved using the embedded "copularnd" function of the MATLAB platform (<https://ww2.mathworks.cn/help/stats/copularnd.html>). If we let the total number of scenarios be SN , the simulated scenarios of lateral inflow of both reservoir n and flood protection region n' can be obtained with the superposition of their deterministic forecasts using Eqs. (8) and (9):

$$Iu_n^s(t) = Iu_n(t)(1 - \varepsilon_n^s(t)), \quad n = 1, \dots, M; \quad t = tc + 1, \dots, tc + T; \quad s = 1, \dots, SN \quad (8)$$

$$Il_n^s(t) = Il_n(t)(1 - \varepsilon f_{n'}^s(t)), \quad n' = 1, \dots, N+1; \quad t = tc + 1, \dots, tc + T; \quad s = 1, \dots, SN \quad (9)$$

The generated fan-structured streamflow scenarios serve as input for risk analysis and decision making for the deterministic and stochastic optimization models.

2.2. Deterministic optimization model for real-time flood water conservation of reservoir systems

Before introducing the MOSP model, the deterministic optimization model that incorporates the determination of the conservation bounds and real-time multireservoir operation (Zhou et al., 2014; Chen et al., 2017) is reviewed and extended to a complex reservoir system. In general, the model framework comprises two steps: 1) determining the

boundary conditions of conservation for each reservoir, and 2) solving the optimization model with the objective of maximizing the conservation benefits based on the bounds and inflow forecasts.

2.2.1. Upper bound of conservation determination through reservoir aggregation and decomposition

The upper bound of the conservation level above the storage of the designed FLWL can be determined as the capacity of the reservoir system available to drawdown the storage during the effective lead time of inflow forecast; therefore, the method is called the “capacity-constrained prerelease method.” For each type of subsystem, the bounds can be determined as described below.

1) Single reservoir system

The upper bound of conservation of reservoir i , $i = 1, \dots, G$ at the beginning of time period td ($Vc_i(td)$) should be constrained by the following equations:

$$Vc_i(td) \leq \sum_{t=td}^{td+Tf_i} [Oc_i(t) - I_i(t)] \cdot \Delta t, \quad td = tc, tc + 1, \dots, tc + T - Tf_i \quad (10)$$

$$Oc_i(t) \leq Omax_i(t). \quad (11)$$

$$If_i(t) = Il_i(t) + P[Oc_i(t - \tau_i), \dots, Oc_i(t)]. \quad (12)$$

$$If_i(t) \leq Qmax_i. \quad (13)$$

where Tf_i is the effective lead time (unit: h) of the inflow forecast of reservoir i , which approximates the average catchment response time; Δt is the time interval (unit: s); and $Oc_i(t)$ and $I_i(t)$ are the reservoir outflow capacity and inflow (unit: m^3/s), respectively, during time period t . Here, $Omax_i(t)$ is the maximum outflow (unit: m^3/s) that can be released from reservoir i during time period t ; $If_i(t)$ is the forecast total inflow (unit: m^3/s) at private downstream protection region i ; $P[\cdot]$ is the flood routing function that calculates the response of the upstream flow at the downstream section after transportation through the river channel; τ_i is the maximum flow delay (unit: h) during routing; and $Qmax_i$ is the maximum safety discharge (unit: m^3/s) of region i .

For a given total forecast inflow where Tf_i is less than the total outflow capacity, Eqs. (10) and (11) indicate that $Vc_i(td) \geq 0$, which means the FLWL can be raised and flood water conservation triggered. Specifically, The equations state that the ending storage beyond effective lead time is controlled to the level of storage of the lower bound of the FLWL, such that flood water conservation does not lower the design standard of the reservoir in relation to flood control. Eqs. (12) and (13) state that the safety of downstream protection region i should be ensured at all times.

2) Cascade reservoirs system

Aggregating a cascade reservoir system as a single “equivalent reservoir” means the total upper bound of conservation of cascade reservoir system j at the beginning of time period td should be confined as follows:

$$\sum_{j'=u(j)}^{d(j)} Vc_{j'}(td) \leq \sum_{t=td}^{td+Tf_j} \left[Oc_{d(j)}(t) - I_{u(j)}(t) - \sum_{j'=u(j)+1}^{d(j)} Iu_{j'}(t) \right] \cdot \Delta t, \quad td = tc, tc + 1, \dots, tc + T - Tf_j \quad (14)$$

$$Oc_{j'}(t) \leq Omax_{j'}(t), \quad j' = u(j), \dots, d(j). \quad (15)$$

$$If_j(t) = Il_j(t) + P[Oc_{d(j)}(t - \tau_{d(j)}), \dots, Oc_{d(j)}(t)]. \quad (16)$$

$$If_j(t) \leq Qmax_j. \quad (17)$$

where j' is the index of the reservoir within subsystem j , ranging from the furthermost upstream reservoir $u(j)$ to the furthermost downstream

one $d(j)$. Here, Tf_j is the effective lead time of the inflow forecast of the entire subsystem, which can be determined as the maximum value of the catchment response time of all member reservoirs for maximizing flood conservation: $Tf_j = \max_{j' \in [u(j), d(j)]} \{Tf_{j'}\}$, or it can be the minimum value of the results of all member reservoirs for ensuring safety: $Tf_j = \min_{j' \in [u(j), d(j)]} \{Tf_{j'}\}$. Parameter $Iu_{j'}(t)$ is the lateral inflow (unit: m^3/s) from the catchment between reservoir j' and its upstream reservoir.

Eqs. (14) and (15) demonstrate that the total upper bound of the conservation level of the system should not exceed the capacity of subsystem j to drawdown the total storage, which is equal to the difference between the water released from the furthermost downstream reservoir ($\sum_{t=td}^{td+Tf_j} Oc_{d(j)}(t) \cdot \Delta t$) and the water flow into the subsystem ($\sum_{t=td}^{td+Tf_j} [Iu_{j'}(t) + \sum_{j'=u(j)+1}^{d(j)} Iu_{j'}(t)] \cdot \Delta t$). This specifies only the constraint on the total conservation level; the constraint on the conservation level of each member reservoir can be disaggregated as follows:

$$Vc_{j'}(td) \leq \sum_{t=td}^{td+Tf_j} [Oc_{j'}(t) - I_{j'}(t)] \cdot \Delta t, \quad td = tc, tc + 1, \dots, tc + T - Tf_j, \quad j' = u(j), \dots, d(j) \quad (18)$$

$$I_{j'}(t) = P[Oc_{\varphi_{j'}}(t - \tau_{j'}), \dots, Oc_{\varphi_{j'}}(t)] + Iu_{j'}(t). \quad (19)$$

where $\varphi_{j'}$ is the index of the reservoir upstream of reservoir j' .

Eq. (18) specifies the limit of the conservation level for each member reservoir associated with its inflow and outflow, while Eq. (19) is the hydraulic continuity equation stating that the inflow of reservoir j' is equal to the summation of the outflow response of its upstream reservoir and the lateral inflow.

The storage complementarity mechanism among member reservoirs can be found when determining the conservation bounds for a cascade reservoir subsystem considering the connection of reservoirs through Eqs. (14) and (18). For example, if a member reservoir were forecasted with high lateral inflow, the FLWL could be lowered to capture the potential flood with a negative conservation limit ($Vc_{j'}(td) \leq 0$). Meanwhile, the upstream member reservoirs could reduce outflow, which would help lower the inflow of the downstream reservoir and increase the conservation limit of the upstream reservoirs ($Vc_{\varphi_{j'}}(td) \geq 0$).

3) Parallel reservoirs system

Similar to the above, the upper bounds of the conservation level of parallel reservoir system k can be determined as follows:

$$Vc_{k'}(td) \leq \sum_{t=td}^{td+Tf_k} [Oc_{k'}(t) - I_{k'}(t)] \cdot \Delta t, \quad td = tc, tc + 1, \dots, tc + T - Tf_k; \quad k' = u(k), \dots, d(k). \quad (20)$$

$$Oc_{k'}(t) \leq Omax_{k'}(t). \quad (21)$$

$$If_k(t) = Il_k(t) + \sum_{k'} P[Oc_{k'}(t - \tau_{k'}), \dots, Oc_{k'}(t)]. \quad (22)$$

$$If_k(t) \leq Qmax_k. \quad (23)$$

where k' is the index of the member reservoir within subsystem k , located on different tributaries of the river system. Eqs. (20), (22), and (23) also demonstrate the storage complementarity mechanism among parallel reservoirs. Given that some member reservoirs can lower their FLWL by increasing outflow, other member reservoirs can raise their FLWL by decreasing outflow, thereby maintaining the total flow at the downstream protection region below the safety threshold.

Finally, as all reservoirs are operated to protect the public protection region F_p , the conservation levels of all reservoirs are coupled to satisfy the limit of the total occupied flood storage to ensure the safety of F_p :

$$\sum_{n=1}^M Vc_n(td) \leq TOS(td), \quad td = tc, tc + 1, \dots, tc + T; \quad (24)$$

where $TOS(td)$ is the limit of the total occupied flood storage at the beginning of time period td , which can be determined for confining the total inflow at F_p below $Q_{max,N+1}$. This constraint links all the subsystems together to obtain suitable combinations of conservation limits.

After decomposing the original complex reservoir system into several isolated or interconnected subsystems falling within the three types, the upper bound of the conservation level of each reservoir during the planning horizon can be derived, providing the storage boundary condition for the real-time operation model. Since the boundary conditions satisfying above equations are possibly non-unique, these equations can be incorporated into the optimization model as constraints for providing combinational conditions.

2.2.2. Deterministic optimization model based on deterministic forecasts

As the purpose of flood water conservation is to reduce the water scarcity risk without increasing the flood risk, the triggering condition should include: 1) precipitation stops and forecast precipitation within planning horizon is nearly zero; and 2) forecast inflow falls below the safety threshold and recedes. The real-time operation of a reservoir system represents an optimization model for seeking informed strategies based on forecasts. A deterministic optimization model uses a single trace of a hydrograph (deterministic forecast) as input, which corresponds to a selected scenario.

(1) Objective function

As deterministic optimization does not directly tackle uncertainty and risk, the objective function is a surrogate for water scarcity risk that sums the water scarcity ratio within the planning horizon $\left(\sum_{t=tc}^{tc+T} \frac{S(t)}{D(t)}\right)$ and the water conservation loss $\left(\frac{Vs(tc+T+1)}{VT}\right)$ at the end of the planning horizon:

$$\min Rs = w_1 \cdot \sum_{t=tc}^{tc+T} \frac{S(t)}{D(t)} + w_2 \cdot \frac{Vs(tc+T+1)}{VT}. \quad (25)$$

$$\sum_{ns \in \Omega} O_{ns}(t) + S(t) - R(t) = D(t). \quad (26)$$

$$\sum_{n=1}^N V_n(tc+T+1) + Vs(tc+T+1) - Vr(tc+T+1) = VT. \quad (27)$$

where $D(t)$ and $S(t)$ are the total water demand (unit: m^3/s) and total water scarcity (unit: m^3/s), respectively, during time period t ; VT and $Vs(tc+T+1)$ are the total active storage (unit: m^3) above the designed FLWL and the total vacant active storage (unit: m^3), respectively, of the complex reservoir system; and w_1 and w_2 are weights to coordinate the water scarcity ratio within $[tc, tc+T]$ and water conservation loss beyond $tc+T$, respectively. The weights, which can be adjusted to determine the priority between water delivery in the current period or water storage for a future period, serve as a factor to influence the hedging effect (Wan et al., 2016). As flood conservation through reservoir operation is implemented during the flood season wherein spillages could frequently occur, w_1 should be greater than w_2 to ensure water delivery rather than conservation. Here, Ω is the set of indices of the furthest downstream reservoirs that deliver water to the users, $O_n(t)$ is the outflow (unit: m^3/s) of reservoir n during time period t ; $R(t)$ is the total water surplus (i.e., spillage; unit: m^3/s) to demand; $V_n(t)$ is the reservoir storage (unit: m^3) at the beginning of time period t (note, all storage variables refer to relative storage above the designed FLWL); and $Vr(tc+T+1)$ is the total surplus storage (unit: m^3).

(2) Constraints

1) Mass balance equation:

$$V_n(t+1) = V_n(t) + [I_n(t) - O_n(t)] \cdot \Delta t, \quad n = 1, \dots, N; \quad t = tc, \dots, tc + T \quad (28)$$

2) Hydraulic continuity:

$$I_n(t) = \sum_{n' \in \varphi_n} P[O_{n'}(t - \tau_{n',n}), \dots, O_{n'}(t)] + \sum_{n' \in \psi_n} P[If_{n'}(t - \tau_{n',n}), \dots, If_{n'}(t)] + Iu_n(t) \quad (29)$$

$$If_i(t) = Iu_i(t) + \begin{cases} \sum_{i' \in \gamma_i} P[O_{i'}(t - \tau_{i',i}), \dots, O_{i'}(t)], & i \neq N+1 \\ \sum_{i' \in \Lambda_{N+1}} P[If_{i'}(t - \tau_{i',N+1}), \dots, If_{i'}(t)], & i = N+1 \end{cases} \quad (30)$$

where ψ_n is the set of indices of flood protection regions located directly upstream of reservoir n ; γ_i is the set of indices of reservoirs located directly upstream of reservoir private protection region i ; and Λ_{N+1} is the set of indices of private flood protection regions upstream of public protection region $N+1$. Specifically, Eqs. (29) and (30) denote the hydraulic continuity of reservoir inflow and river channel inflow, respectively.

3) Storage limits:

$$Vd_n(t+1) \leq V_n(t+1) \leq Vc_n(t+1), \quad t = tc, \dots, tc + T \quad (31)$$

where $Vd_n(t+1)$ is the lower bound of the ending storage (unit: m^3) at time period t for reservoir n .

4) Outflow limits:

$$Omin_n(t) \leq O_n(t) \leq Omax_n(t), \quad t = tc, \dots, tc + T \quad (32)$$

where $Omin_n(t)$ is the minimum outflow requirement (unit: m^3/s) during time period t on reservoir n .

5) Initial condition:

$$V_n(tc) = VI_n \quad (33)$$

where VI_n is the beginning storage volume (unit: m^3/s) of reservoir n .

6) Safety for protection region

This constraint is characterized in Eqs. (13), (17), (23), and (24) for different types of subsystem and for the entire system.

The introduced model requires inputs of the initial conditions of storage from observation, boundary condition from the simulation module described in Section 2.2.1, and deterministic forecasts of inflows, as described in Section 2.1.3. After solving the model, the outflow and storage strategies of flood water conservation for each reservoir and the hydrograph of each flood protection region can be obtained simultaneously.

2.3. Real-time MOSP for flood water conservation of a multireservoir system under uncertainty

With the simulated streamflow scenarios, the real-time MOSP is proposed to conduct multiobjective risk optimization for flood water conservation under uncertainty.

2.3.1. Multiple objectives under uncertainty

Rather than separating flood water conservation processes to bound determination and real-time optimal operation, MOSP does not derive dynamic storage bounds. Instead, it formulates directly the conflicting objectives of upstream flood risk, downstream flood risk, and water scarcity risk as a multiobjective optimization problem and it determines a strategy for compromise. Specifically, as uncertainty is addressed, all the risk indices are evaluated at the mean value of the outcomes under discretized uncertain streamflow scenarios, and the stochastic programming model can be converted to its deterministic equivalent. The

water scarcity risk ($E[R_s]$) is the expected value of the synthesized water scarcity ratio and water conservation loss. The upstream flood risk ($E[R_u]$) is measured by the expected value of the total loss ratio of flood protection storage, which calculates the summation of the loss ratio of all reservoirs. The downstream flood risk ($E[R_d]$) is evaluated by the expected value of the total loss ratio of the peak flow to the maximum safety discharge of the protection regions, which is the summation of the loss ratio of all protection regions. It can be discerned that $E[R_u]$ and $E[R_d]$ represent the surrogate loss of flood events caused to the reservoir system and the downstream protection regions (Zhu et al., 2018), respectively. Accordingly, the objectives can be characterized as follows:

$$\text{Min}(E[R_s], E[R_u], E[R_d]) \quad (34)$$

Objective I:

$$E[R_s] = \sum_{s=1}^{SN} pr^s \left[w_1 \sum_{t=tc}^{tc+T} \frac{S^s(t)}{D(t)} + w_2 \frac{Vs^s(tc+T+1)}{VT} \right] \quad (35)$$

Objective II:

$$E[R_u] = \sum_{s=1}^{SN} pr^s \sum_{n=1}^M \max_{t \in [tc, tc+T+1]} \{V_n^s(t)/V_{\max,n}(t)\} \quad (36)$$

Objective III:

$$E[R_d] = \sum_{s=1}^{SN} pr^s \sum_{n'=1}^{N+1} \max_{t \in [tc+1, tc+T]} \{I_n^s(t)/Q_{\max,n}\} \quad (37)$$

where pr^s is the probability of streamflow scenario s , and $V_{\max,n}(t)$ is the flood protection storage (unit: m^3) of reservoir n . Under the influence of uncertainty, all variables related to reservoir operations include a superscript s , denoting the value under scenario s .

2.3.2. Constraints

For determining a robust strategy feasible for all considered scenarios, all the constraints introduced in the deterministic model are now bound to the stochastic decision and state variables, based on the simulated streamflow scenarios. Moreover, the upper bound of storage is changed to $V_{\max,n}(t)$ within the storage limit constraint given in Eq. (31). It is because the effect of the limitation on intermediate variables of the upper conservation bound is already considered in MOSP by the optimization of the flood risk objectives.

In the MOSP model, the time periods are usually divided into two categories: the current period (here and now) and forthcoming periods (wait and see). To address the linked influence of future inflows on the release of the current period, nonanticipativity constraints are imposed on the release decision:

$$O_n^{s_1}(tc) = O_n^{s_2}(tc) \quad \forall s_1, s_2 \in [1, SN] \quad (38)$$

2.3.3. Noninferior solutions generation

The three objectives considered are mutually conflicting because reducing the water scarcity risk encourages flood water conservation, which increases surplus water that could enhance either the upstream or the downstream flood risk. Consequently, no single solution can simultaneously optimize all the objectives; therefore, only noninferior solutions that satisfy Pareto optimality can be obtained. The noninferior solution set provides decision makers with abundant candidate choices with various levels of objectives. A mature and common approach to obtain representative noninferior solutions is the ε -constraint method (Haimes, 1977) that converts multiobjective optimization into single objective optimization through transforming partial objectives to ε -constraints, which leaves only one objective to be optimized:

$$\text{Min } E[R_s] \quad (39)$$

Subjected to

$$E[R_s] \leq \eta_{Rs} \quad (40)$$

$$E[R_d] \leq \eta_{Rd} \quad (41)$$

where η_{Rs} and η_{Rd} are the constraint bounds for the upstream and downstream flood risks, respectively. The conversion can be interpreted as obtaining a solution with $E[R_s]$ and $E[R_d]$ being limited to below η_{Rs} and η_{Rd} , respectively, which caters for the decision requirement for determining the optimized conservation strategy under acceptable risk levels.

With decreases in the values of η_{Rs} and η_{Rd} , the solutions become conservative on flood water conservation because the allowable flood risk level is tightened. For obtaining representative and numerous noninferior solutions, one can first identify the variation bounds of η_{Rs} and η_{Rd} by single objective optimization with ε -constraints relaxed, and then set groups of constraint bounds within the variation range to solve.

2.4. Recourse decisions within a rolling horizon

Considering the influence of forecast error in decision making provides opportunity to inform decisions with favorable and unfavorable scenarios at hand. However, this does not guarantee that the operation process is absolutely secure. When the confidence range of scenarios does not accurately cover the actual streamflow processes, risks may occur. To correct a possibly incorrect decision made in the previous time period and its negative consequence, attributable to biased information, a recourse action is taken in the subsequent time period based on the updates. This is proceeded in a dynamic rolling horizon with information and decisions frequent change.

Differences in the deterministic and stochastic optimization models exist primarily in relation to tackling uncertainty and risk. As deterministic optimization can deal with only one particular scenario at a time, risk analysis coupled with a trial-and-error approach should be employed for rationalizing decisions in the current time period. This should include the following steps:

- 1) optimize the operation strategy based on the deterministic forecast;
- 2) optimize the operation strategies for each of the generated scenarios while minimizing the deviation in the current release with that of the operation strategy based on the deterministic forecast;
- 3) examine whether the risk indices of the outcomes based on the scenarios and forecasts are within tolerance levels; if not, add constraints to alter the release strategies to lower the risks, and return to step 1).

In contrast, MOSP directly applies risk constraints and grandly optimizes the release strategies under all scenarios and forecasts. Therefore, the constraint level in MOSP is sufficiently tight to ensure overall robustness of the obtained strategies. Moreover, MOSP pursues a better statistical objective in terms of grand optimization. Consequently, a strategy obtained by deterministic optimization could be inferior to that of MOSP, particularly in terms of risk aversion.

For highlighting the effect of recourse decisions, a third model with no recourse decisions is introduced. With the no recourse situation, decision variables are fixed even if uncertainty is realized. This is a deterministic optimization model which “neglects” uncertainty when making a decision, i.e., considering only the expected value information. The corresponding solution is named as expected value solution (solution E). However, this does not mean uncertainty is absent. The evaluation of solution quality in each scenario or in real-time situations still counts uncertainty in.

After implementation of current release decisions, the transit status and other information of a reservoir update as time evolves. Simply, let $tc \leftarrow tc + 1$ and run the models again with updated forecasts and simulated scenarios. The simulated actual release and storage trajectories from the three models are compared after implementing the strategies

for specific time periods.

2.5. Solution algorithm

The models are solved using the generalized reduced gradient method (Lasdon et al., 1974) for the general structure of nonlinear programs, given that the characteristic curves of the reservoirs and flood protection regions could be fitted by continuous and differentiable nonlinear functions. Lasdon et al., (1974) provided and proved the details of the algorithm. The algorithm was developed using a globally commercial solver (LINGO), which can be downloaded at <http://www.lindo.com>. To enhance the chance of reaching a global optimum, each formulated model was solved using multiple initial solutions and the best optimal solution among these initial starts was determined.

3. Overview of the multireservoir system

The Pi River Irrigation District, which is located on one of the tributaries of the Huai River, is part of China's second largest irrigation district (i.e., the Pishihang Irrigation District), incorporating a total irrigation area of $73.33 \times 10^4 \text{ hm}^2$. Primary irrigation water is delivered from a multireservoir system that includes the Bailianya (BLY), Mozitan (MZT), Foziling (FZL), and Xianghongdian (XHD) reservoirs located on the upstream reaches of the Pi River. The location and topological structure of the mixed reservoir system is shown in Fig. 3. Irrigation water is delivered mainly during the period May–October, which is both the growth season of rice and the flood season of the reservoir system. The demand for irrigation water is high during the dry inflow period (July–August) after the monsoon rains terminate. Currently, the reliability of irrigation water supply is 73% and the efficiency of water resource utilization is only 50%. Statistics show that the estimated annual water shortage in this area is 145 million m³.

In addition to the objectives of domestic and agricultural irrigation

Table 1
Characteristics and parameters of the reservoirs system.

Content	BLY	MZT	FZL	XHD
Drainage area (km ²)	745	570	525	1400
Active storage (million m ³)	21.3	69.2	141.1	185.9
Flood protection storage (million m ³)	28	111	95	486
Lower bound of ending storage (million m ³)	-40	-40	-40	-40
Total water demand (m ³ /s)	—	—	120	120
Maximum safety discharge of downstream region (m ³ /s)	—	—	3450 ^a	2500 ^b
Effective leading time of inflow forecast (h)	3	3	2	5
Maximum flow delay (h)	1	1	0 ^d /5 ^e	0 ^d /5 ^e

^{a,b, c} Maximum safe discharge of Huoshan, Dushan, and Lu'an, respectively.

^dHuoshan and Dushan are located close to FZL and XHD, respectively, such that the flow delay is zero.

^eThe maximum flow delay from Huoshan to Lu'an and from Dushan to Lu'an.

water supply, the major purpose of the reservoir system is to protect the safety of three downstream cities during the flood season, i.e., Huoshan (HS), Dushan (DS), and Lu'an (LA). HS and DS are located close to FZL and XHD, respectively; the flow delay from each reservoir to its nearest downstream city is less than 1 h. The maximum delay for water flow from HS to LA and from DS to LA are both 5 h, and the routing function can be characterized as a linear function with coefficients calibrated by the least squares method. Owing to the limitations of the current operational rules and the Chinese Flood Control Act, the water level of the reservoir system is strictly controlled to below the designed FLWL before the flood period, resulting in spillage of 1545 million m³/a. Actually, the reservoir system was constructed with a total active storage above the designed FLWL (VT) of 417 million m³. Frequently, a high level of vacant active storage is preserved for the purpose of flood control, which raises strong conflict between the demands for flood control and water supply. Details of the basic characteristics of the

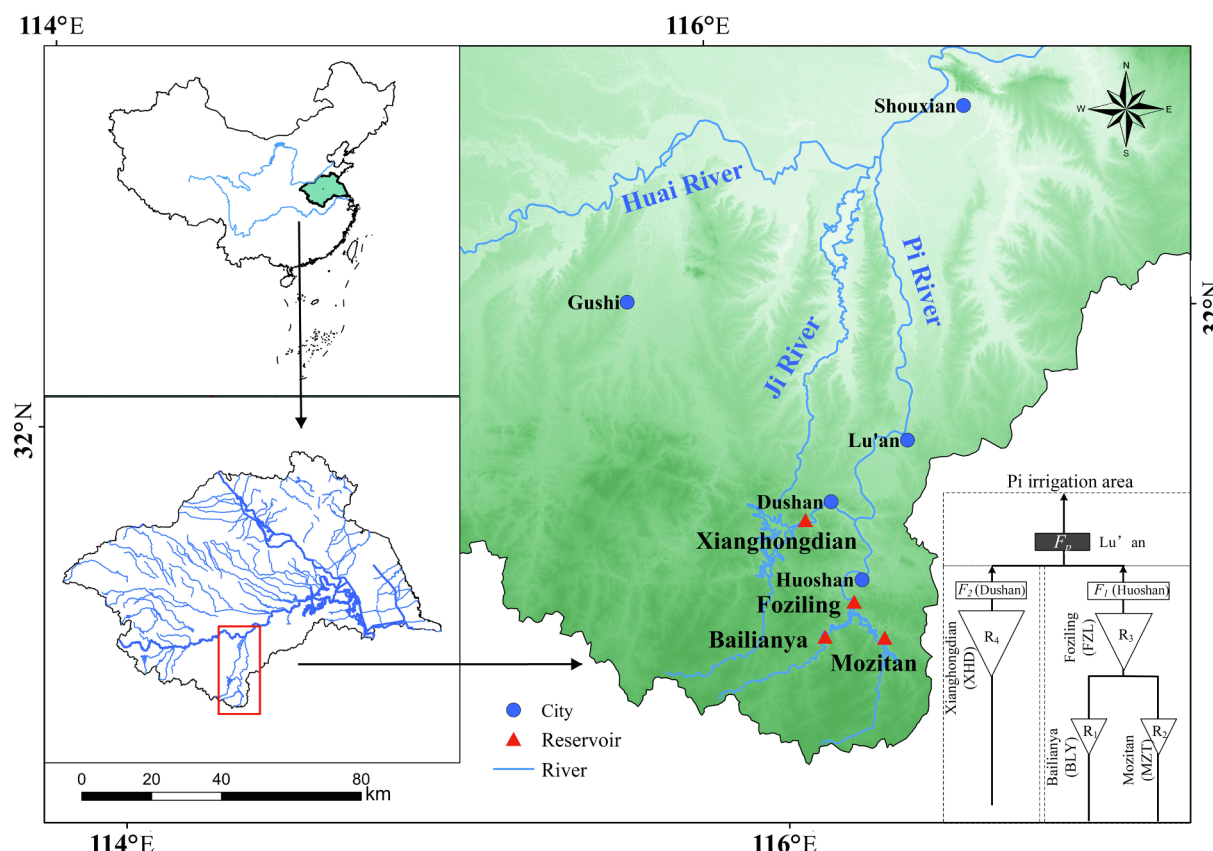


Fig. 3. Sketch map and location of the multireservoir system in the Pi River Basin.

reservoir system are provided in Table 1.

The studied region is located in the transitional zone between humid and semiarid climates, where storms and drought occur frequently and alternately as responses to the transition of weather conditions (Wu et al., 2017). Regular operation of the reservoirs for flood control is supported by rainfall and flood information monitoring, together with forecasting systems with real-time response. The system, which is driven by the inputs of observed rainfall and a numerical weather forecast (1-d ahead) released by the meteorological department of China (Cai et al., 2018a, 2018b), provides hourly automatic forecasts of streamflow for the entire reservoir system with a rolling 24-h window based on the Xinjiang flood forecast model (Zhao 1992).

A typical receding flood event that commenced at 06:00 local time on August 10, 2015 and ended at 12:00 local time on August 14, 2015 was selected for simulating the flood water conservation strategies of the two models within the rolling horizon. First, experiments were conducted for planning the 24-h conservation strategy at the time at which the flood water began to recede with uncertain streamflow scenarios. To highlight the differences in operational strategies, the two models were both run and the deterministic model solution was compared with the noninferior solution set of MOSP. Thereafter, real-time implementation of the operational strategies of the two models was simulated in a rolling horizon.

4. Case study

4.1. Scenario generation using the copula function

Synthetic scenarios of streamflow were generated to reflect forecast uncertainty using the t copula function with parameters calibrated from the sample data of forecast and actual streamflow records. Here, SN was calibrated as 40 with the purpose of preserving most of the statistical moments and correlations. Statistical tests revealed insignificant correlation between the forecast errors of the downstream lateral inflow of the public protection regions and that of the upstream reservoirs; however, significant correlation was detected among the forecast errors of the streamflow of the upstream reservoirs. The spatial and temporal correlation coefficient matrices for the actual data and the simulation results for streamflow forecast errors among the four reservoirs are shown in Fig. 4(a) and (b), respectively.

It can be seen that the effect of the temporal correlation dominates that of the spatial correlation owing to the strong relationship between streamflow response and precipitation input, i.e., biases in precipitation forecasts would propagate through a rainfall-flood forecast model and influence sequences of forecast error on temporal scales. Moreover, strong positive spatial correlation with forecast errors can be found. This is because the entire river basin of the reservoir system is small, and weather conditions as well as precipitation are mostly synchronized within the subsystems. Overall, the results show that the t copula function can preserve the correlations, despite the partial differences from the actual data in low-correlation situations.

Fig. 5 shows the range of confidence of the simulated scenarios of streamflow for the system within the rolling horizons. For clear demonstration, only some of the rolling simulations are presented.

Results show that although the simulated scenarios cover the actual streamflow processes for most cases, discrepancies do increase with forecast lead time. The hit rate of the 1-d forecasts for no-rainfall events (precipitation ≤ 0.1 mm) for this system reaches 85.9%, i.e., the chance of a missing alarm that could result in excessive flood water is nearly 14%. Flood water conservation was triggered at the beginning of the studied event because the forecast total inflow fell rapidly below the water demand after August 11; otherwise, water scarcity would have occurred. The simulated scenarios underestimate the receding floods, resulting in overestimate of water scarcity risk. The negative influence of biases can be corrected by rolling horizon adaptation through reservoir operation. Forecast verification of more events can be checked

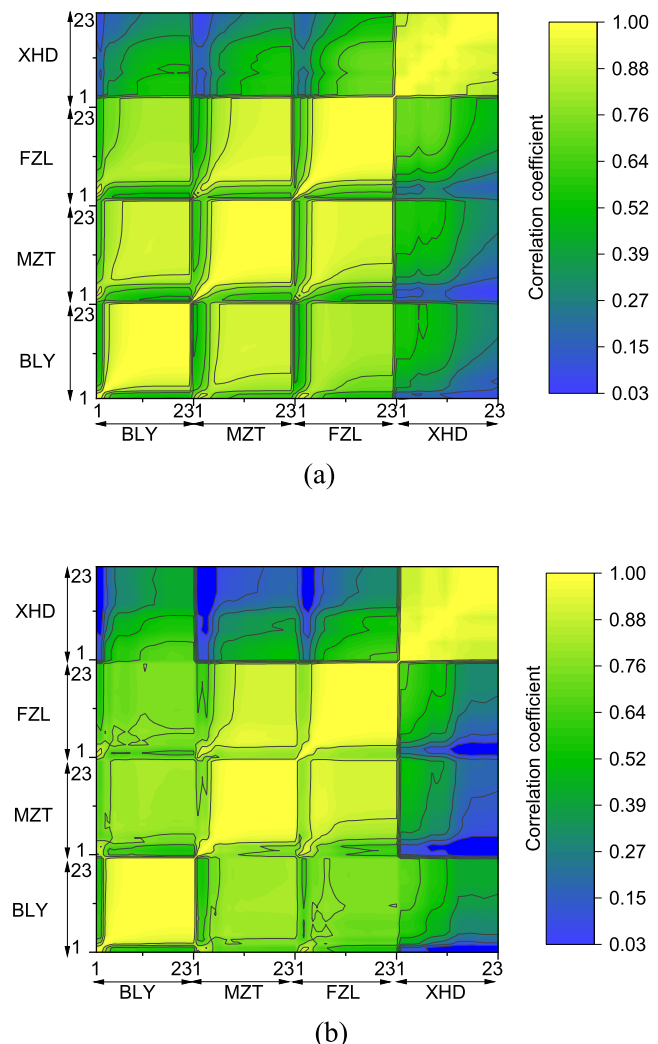


Fig. 4. Spatial and temporal correlation matrix for streamflow forecast errors of the four reservoirs: (a) actual data and (b) simulated results based on the t copula function.

at supplementary note.

4.2. Real-time optimal solutions for flood conservation

4.2.1. Model results of objectives

Setting the weights $w_1 = 0.7$ and $w_2 = 0.3$ through analysis, the deterministic model solution (solution D, i.e., a benchmark solution) was obtained with the inputs of the generated scenarios and the boundary conditions to derive the first 24 h operational plan. Meanwhile, the noninferior solutions from MOSP were also obtained through the ϵ -constraint method. The objectives of the Pareto front and solution D are shown in Fig. 6. It should be noted that expected water conservation loss was used to evaluate the effect of flood water conservation. This was because the expected water scarcity ratio of all solutions was zero owing to the higher priority given to water delivery during the planning horizon. Two specific noninferior solutions were selected from the front: 1) solution SI (a low water-scarcity-risk solution), obtained with the objective of minimizing $E[R_s]$ with the same constraints on $E[R_u]$ and $E[R_d]$ as the corresponding results of solution D; and 2) solution SII (a low upstream-flood-risk solution), derived with the objective of minimizing $E[R_u]$ with the same constraints on $E[R_s]$ and $E[R_d]$ as the values of solution D. Solutions SI, SII and solution E were systematically compared with solution D.

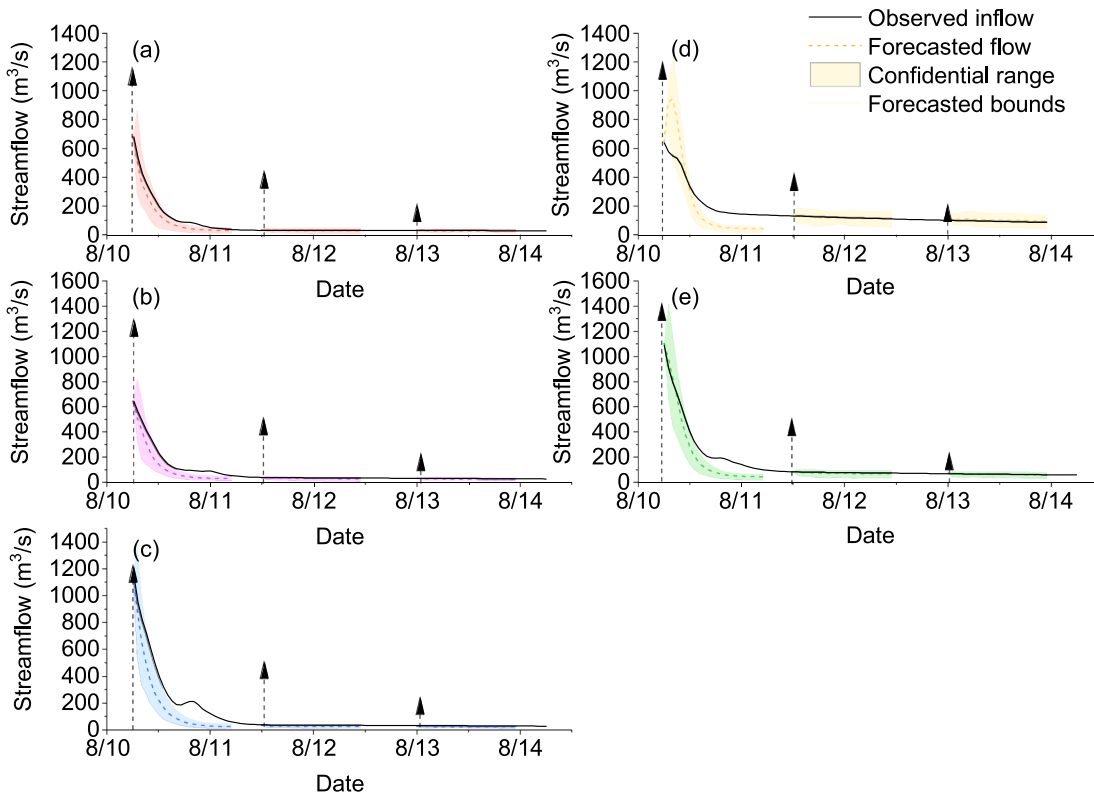


Fig. 5. Rolling streamflow forecasts and simulated scenarios of the reservoir system during the stage of receding flood 20150810: (a) BLY, (b) MZT, (c) FZL, (d) XHD, and (e) the downstream lateral inflow.

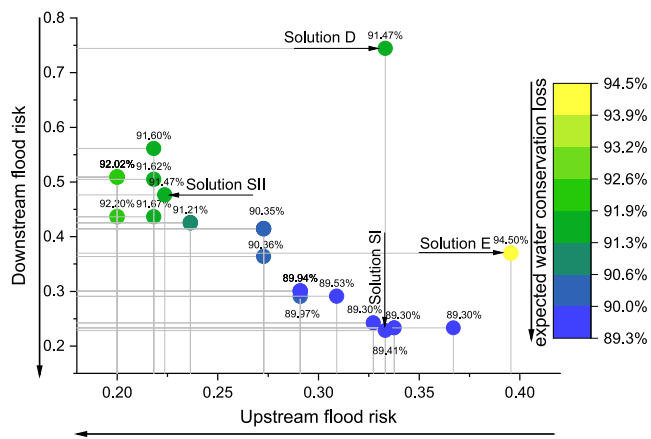


Fig. 6. X-Y projection of noninferior solutions and solution D.

Conflicting decisions among the Pareto front can be identified for flood water conservation levels in the range of [7.8%, 10.7%] (i.e., conservation loss in the range of [89.3%, 92.2%]) of active storage, resulting in variation in the upstream flood risk at [0.2, 0.37] and downstream flood risk at [0.22, 0.56]. To reduce water scarcity risk through flood water conservation by selecting a noninferior solution, either the upstream flood risk increases in the X-axis direction or the downstream flood risk increases in the Y-axis direction. Evidently, solutions SI and SII dominate solutions D and E, indicating the performance of MOSP is superior to that of the deterministic optimization model and expected value solution. Specifically, Table 2 summarizes the statistics of the four solutions.

In comparison with the benchmark solution D, the derived results reveal the following.

- Solution I lowers the expected conservation loss by 2.06% without

Table 2
Decision and objective values of the four solutions.

Solution type	Solution D	Solution SI	Solution SII	Solution E
Expected value of water scarcity ratio	0	0	0	0
Water conservation loss	91.47%	89.41%	91.47%	94.50%
Total conservation level (Ending storage) (Million m ³)	35.62	44.66	35.62	26.34
BLY (R ₁)	-2.90	-6.89	-2.87	1.63
MZT (R ₂)	-3.53	10.71	9.80	2.62
FZL (R ₃)	25.78	18.07	8.93	13.17
XHD (R ₄)	16.28	22.77	19.77	8.93
Upstream flood risk	0.33	0.33	0.22	0.4
(%)	(-33%)	(-33%)	(-33%)	(20%)
BLY (R ₁)	0.00	0.00	0.00	0.20
MZT (R ₂)	0.00	0.10	0.09	0.02
FZL (R ₃)	0.29	0.19	0.09	0.15
XHD (R ₄)	0.04	0.05	0.04	0.02
Downstream flood risk	0.74	0.23	0.48	0.37
(%)	(-69%)	(-36%)	(-50%)	
HS (F ₁)	0.38	0.07	0.25	0.18
DS (F ₂)	0.08	0.00	0.03	0.15
LA (F ₃)	0.28	0.16	0.20	0.04

*Percent values in parentheses indicate the variation compared with the results of solution D.

increasing the flood risk. The reduction in water scarcity risk in comparison with solution D corresponds to an increase in expected total ending storage of 9.04 million m³. This is attributable primarily to the effect of multiobjective optimization on the spatial conservation plans of the system. Solution D conserves more water in the FZL subsystem than in the XHD subsystem because the safety discharge capacity of HS is greater than that of DS ($Q_{max_1} \geq Q_{max_2}$), which means the FZL subsystem could pre-release more water under the emergent cases. This solution

- weakens the influence of reservoir storage regulation. In contrast, solution I increases water conservation in XHD because this reservoir has the largest flood protection storage, which results in the lowest upstream flood risk from flood water conservation. Therefore, solution I explores higher potential utility of flood water conservation than solution D.
- (ii). Solution II reduces the upstream flood risk by 0.11 without increasing the downstream flood risk or the water scarcity risk. The decrease in the upstream flood risk is also attributable to an appropriate balance among the objectives from MOSP. Minimizing $E[R_u]$ encourages increased conservation in both XHD and MZT and decreased conservation in FZL because XHD and MZT have greater flood protection storage than FZL and BLY. Consequently, a more homogenized upstream flood risk is obtained by solution II than by solution D and this homogenization helps lower the total risk.
 - (iii). Both noninferior solutions exhibit lower downstream flood risk than solution D. This is because the deterministic optimization model does not address directly the minimization of the downstream flood risk. The model assumes that the ability to release surplus water to the downstream river channel buffers the upstream flood risk of conservation.
 - (iv). Solutions with recourse take the advantage of adapting and correcting the influences of uncertainty, which yield superior performance in flood water conservation and risk control than solution without recourse. Results of solution E conserves the lowest flood water at the expense of a highest upstream flood risk and a medium level of downstream flood risk, demonstrating the importance of multiple scenario analysis and recourse decisions in improving decision making and risk aversion.

The risk objectives were evaluated using the expected value of the corresponding indicator for all considered scenarios, which only reflects the mean outcome. Fig. 7 shows the histogram distribution of the objective value under uncertain scenarios. It demonstrates that the improved performance in lowering water scarcity risk by solution I, in comparison with stochastic programming, is achieved because of its flexibility in conserving flood water through grand optimization under divergent scenarios. Although it conserves a greater volume of flood water, it transfers downstream risk to upstream risk via the capture of surplus water within the storage. Moreover, the reduction in upstream flood risk by solution II stems from a superior compromise among upstream and downstream risks. Although solution II yields the same $E[R_s]$ as solution D, its greater variation in distribution indicates possible severe water scarcity under extreme dry scenarios. This is because the current MOSP model is constrained only on the mean model response, i.e., without restriction under each specific scenario or extreme scenarios. Due to the inability of regulating reservoir operation performances via recourse decisions, solution E yields the most flatten distribution of water conservation loss and upstream flood risk.

4.2.2. Comparison of solutions

Differences in reservoir storage and outflow trajectories among the three solutions are depicted in Figs. 8 and 9, respectively. In general, the variation in storage indicates the cumulative influence on storage uncertainty through risk propagation. The storage complementarity mechanism of the FZL subsystem can be identified in solution D: the storage of both BLY and MZT is operated below the FLWL, while the storage of FZL is kept high for conservation. Solutions I and II simultaneously address the storage complementarity mechanism within and between the reservoir subsystems. They sufficiently explore the use of the high storage capacity of XHD to conserve flood water and allocate more conservation to MZT than to FZL to lower the total risk. This is because conservation in XHD and MZT corresponds to only 5% and 10%, respectively, of their storage capacities, whereas that of FZL would be 20%. Using the least cost of the upstream flood risk to hedge

the cost of the water scarcity risk in the future, it can be determined that solutions I and II dominate solution D and solution E. Moreover, the downstream flood risk is reduced substantially through MOSP within the grand optimization.

4.3. Dynamic rolling horizon decision making with recourses

Considering the influence of forecast uncertainty on actual decision-making processes, a rolling horizon simulation with recourses was conducted with real-time updates of information and strategy. With only the decision in the current time period implemented, Tables 3 and 4 list the simulated snapshots of actual operation processes results of the reservoirs and the downstream regions among the four solutions, respectively.

Within the entire horizon, all solutions partially conserve flood water and raise reservoir storage at the beginning, and then drawdown the storage to deliver the conserved water as the inflow decreases. Using XHD for conservation, Solution I conserves 4.86 million m^3 (12%) more water at the end of the period with 1.6% less upstream flood risk than solution D. Solution II reduces the upstream flood risk by 3.1% in comparison with solution D with the same level of water conservation. This is because the homogenization of the upstream flood risk among the reservoirs constitutes a lower total risk. Meanwhile, the maximum downstream flood risk of the two noninferior solutions is also controlled to below that of solution D. Additionally, solution E is dominated by solution SII.

Although notable reduction in the total risk can be identified within the planning horizon when using MOSP, owing to the limitation of depicting inflow and precipitation results beyond the planning horizon (Zhao et al., 2012), the effect of flood risk control beyond the planning horizon cannot be ensured directly. This means that the spatial allocation at the end of flood prevention storage by the reservoir system cannot be identified as the best initial storage plan beyond the horizon. This limitation affects all similar reservoir operation models. One possible extended technique to improve the utility of MOSP in this case would be to incorporate multicriteria decision making, which allows decision makers to select a compromise solution from the noninferior solution set, catering for subjective preferences in terms of criteria and the objective environment that affect dynamic decision making. As such, potential remains for further development of the proposed approach.

5. Discussion

Historical receding flood events during year 2014 to 2016 were examined with rolling horizon experiments were conducted on the solutions. Table 5 lists the results of flood water conservation, and comparisons are investigated with solution D setting as a benchmark.

Results indicate that solution SI from MOSP outperforms solution D and solution E in terms of flood water conservation without increasing flood risks. Compared to solution D, the mean increase in flood water conservation from MOSP is 2.49 Million m^3 per flood (9.3%), and the increase approximates positive correlation to the receding water volume. This is because MOSP explores better optimization effect within a wider solution space. On the other hand, compared with solution D, the mean decrease in flood water conservation from solution E is 7.93 Million m^3 per flood (29.7%), indicating that recourse decisions are rather effective in improving solution optimality, especially when receding flood water volume is high.

6. Conclusions

This study proposed a multiobjective stochastic programming model to inform real-time operation of flood water conservation in a multi-reservoir system under uncertainty. Inflow uncertainty was characterized as the spatial and temporal correlated forecast error processes with

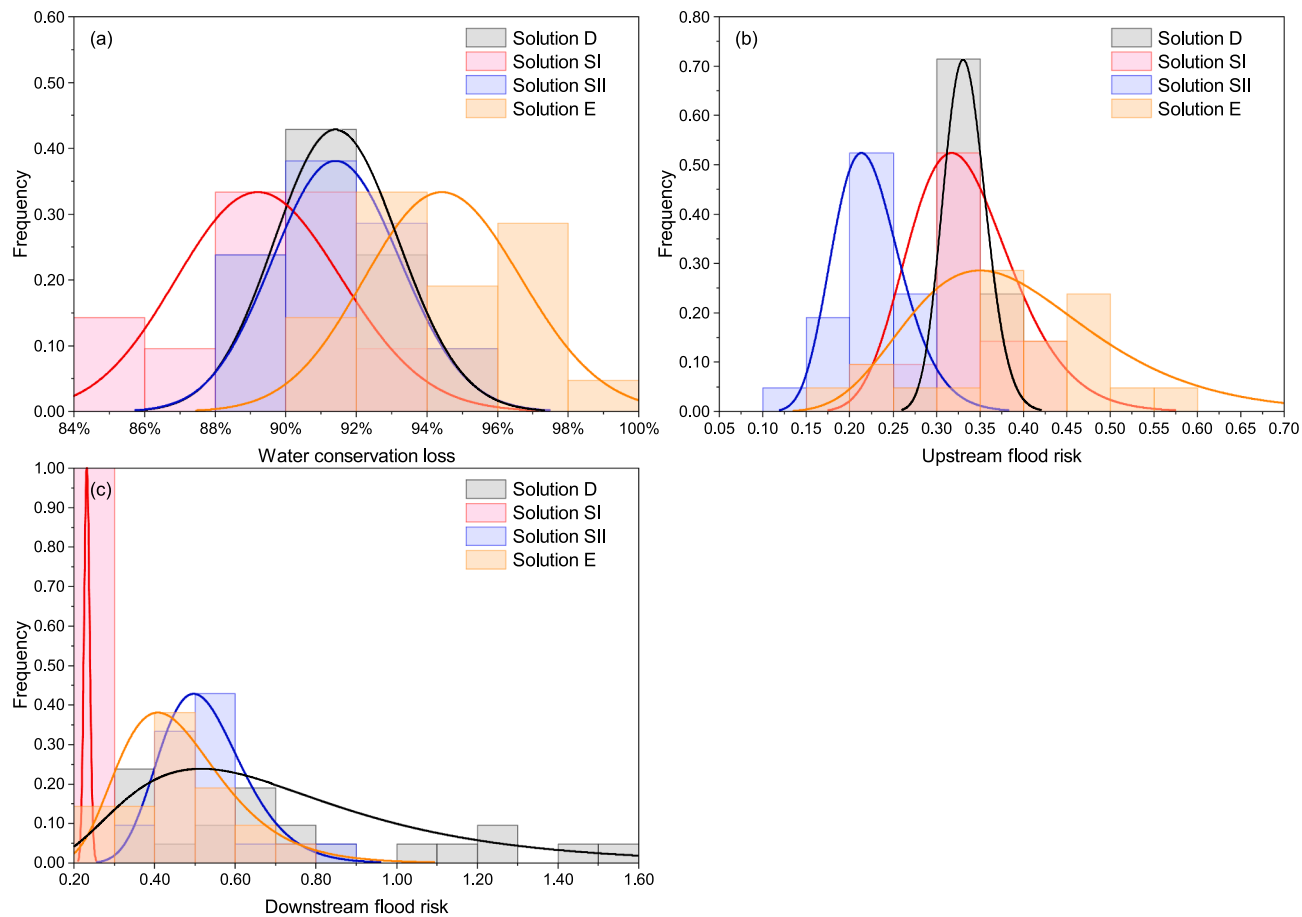


Fig. 7. Objective results under uncertainty and different solutions.

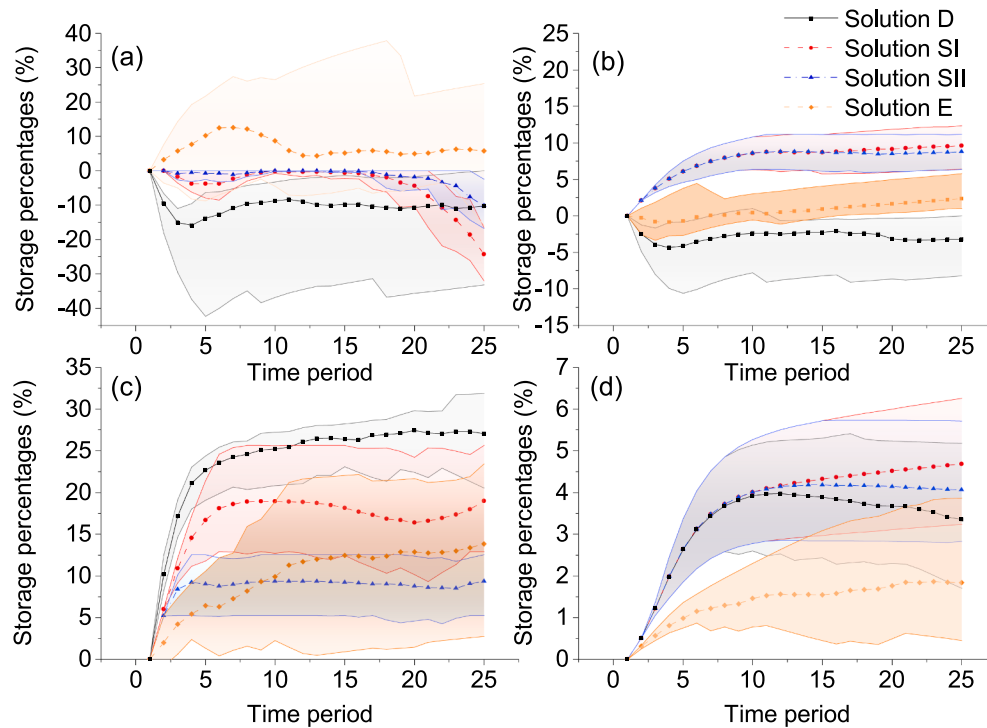


Fig. 8. Reservoir storage trajectories and range of confidence.

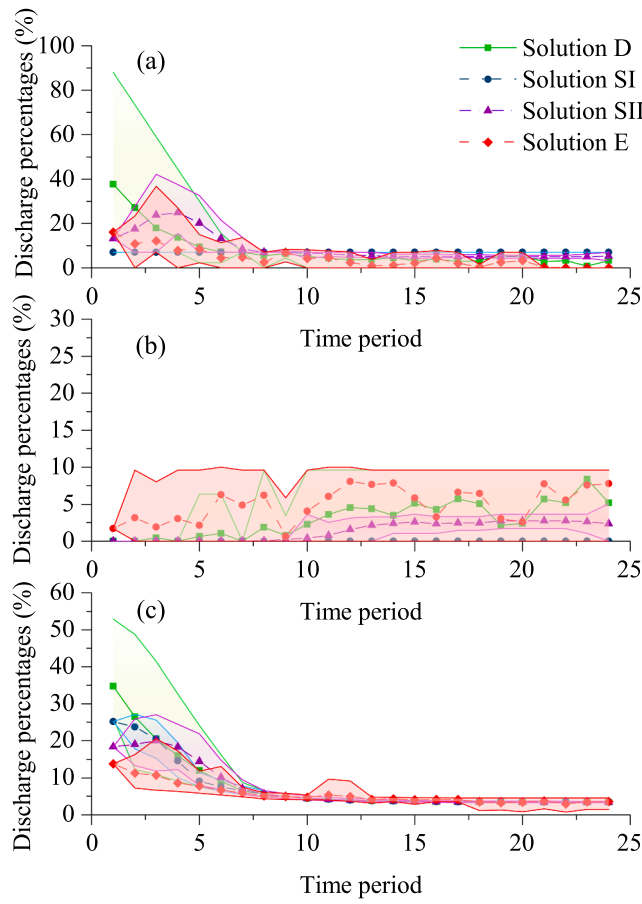


Fig. 9. Discharge trajectories and range of confidence for flood control points.

a joint probability density function modeled using a copula function. Discretized inflow scenarios of the reservoir system served as input for the multiobjective stochastic programming with the objective of minimizing water scarcity risk, as well as the upstream and downstream flood risks of the entire reservoir system. A rolling horizon with recourse for real-time operation updating was modeled to address the dynamic decision-making characteristics. Experiments were conducted on the mixed reservoir system of the Pi River Basin in China. The main findings derived were as follows.

- (1) Capturing the dependencies of forecast uncertainty within the reservoir system using a copula function could address the spatial and temporal continuity relation of inflow forecast, which provided informative forecast support for real-time reservoir operations.
- (2) Noninferior solutions obtained from MOSP, which dominate the deterministic optimal solution, can either conserve 4.86 million m³ (12%) more water without increase in the upstream and downstream flood risks, or reduce the upstream flood risk by 3.1% without increase in water scarcity and downstream flood risk during the receding flood of 20150810.
- (3) MOSP provides coupled grand optimization and dynamic decision making to find robust solutions among multiple risks. Groups of noninferior solutions could be selected according to various decision-making environments.

The proposed MOSP could efficiently mitigate the risks raised by forecast uncertainty, and the efficiency of risk reduction depends on the characterization accuracy of risk sources. This study applies the copula function to address total forecast uncertainty from precipitation forecast to hydrological forecast based on statistics of error samples. The proposed methodologies could also be driven by multiple forecasts

Table 3
Flood water conservation results among the three solutions in a rolling horizon simulation.

Date	Solution D	Solution SI						Solution SII						Solution E						
		BLY	MZT	FZL	XHD	BLY	MZT	FZL	XHD	BLY	MZT	FZL	XHD	BLY	MZT	FZL	XHD	Conservation (million m ³)		
10-Aug	0.0%	0.0%	0.0%	0.0%	0.0%	0.0%	0.0%	0.0%	0.0%	0.0%	0.0%	0.0%	0.0%	0.0%	0.0%	0.0%	0.0%	0.00	0.00	
10-Aug	-10.1%	-3.0%	23.6%	3.5%	33.23	-1.8%	7.5%	9.1%	3.38	-1.6%	7.5%	9.1%	3.5%	33.40	-5.5%	-2.0%	15.8%	3.3%	27.46	
10-Aug	-3.9%	-1.3%	25.6%	5.1%	46.74	-0.1%	10.0%	11.4%	5.2%	0.0%	10.0%	10.7%	5.2%	46.70	-3.1%	-0.1%	21.1%	4.5%	40.86	
11-Aug	-3.2%	-1.0%	26.4%	5.7%	50.63	-1.2%	11.3%	11.8%	6.1%	53.17	-0.1%	10.0%	10.6%	6.0%	50.47	-2.3%	0.1%	24.4%	4.9%	44.62
11-Aug	-3.0%	-1.0%	26.7%	5.8%	51.82	-1.9%	12.3%	11.1%	6.5%	55.23	-0.5%	9.8%	10.0%	6.5%	51.79	-3.5%	-1.8%	24.6%	5.2%	45.66
11-Aug	-2.3%	-0.7%	26.8%	5.7%	52.00	-2.2%	12.7%	9.9%	6.7%	55.44	-0.5%	9.8%	9.8%	6.6%	51.98	-6.9%	-2.7%	26.1%	5.3%	45.73
11-Aug	-2.5%	-1.1%	26.6%	5.8%	51.67	-2.7%	13.1%	8.5%	6.8%	55.11	2.0%	10.3%	6.8%	6.8%	51.65	-8.9%	-2.1%	25.5%	5.4%	45.41
12-Aug	-3.5%	-0.7%	26.8%	5.7%	51.22	-3.1%	13.5%	7.8%	6.9%	54.86	1.8%	10.1%	6.5%	6.9%	51.33	-6.6%	-1.5%	25.5%	4.9%	44.65
12-Aug	-4.1%	-0.7%	25.7%	5.8%	50.69	-2.3%	13.3%	6.0%	7.1%	54.32	1.5%	10.0%	6.3%	6.8%	50.75	-5.0%	-1.2%	22.1%	5.3%	44.10
12-Aug	-4.0%	-0.8%	25.9%	5.6%	50.05	-2.2%	13.2%	4.3%	7.3%	53.72	1.0%	9.9%	6.1%	6.8%	50.12	-6.8%	-1.2%	23.2%	5.0%	42.97
12-Aug	-2.8%	-0.9%	25.3%	5.5%	49.14	-2.1%	13.7%	2.1%	7.4%	52.80	0.4%	9.7%	5.8%	6.7%	49.16	-5.9%	-1.4%	23.5%	4.6%	41.47
13-Aug	-2.1%	-0.6%	23.1%	5.7%	48.26	-3.5%	14.3%	0.2%	7.6%	51.93	-0.1%	9.5%	5.4%	6.7%	48.28	-4.7%	-1.3%	22.6%	4.5%	40.47
13-Aug	-2.1%	-0.3%	21.2%	5.8%	47.27	-1.8%	14.8%	-3.3%	7.8%	50.91	-0.6%	9.3%	5.2%	6.6%	47.27	-4.0%	-1.0%	22.7%	4.1%	39.36
13-Aug	-3.2%	-0.4%	21.7%	5.6%	46.38	-6.3%	15.3%	-4.8%	8.1%	50.03	-1.1%	9.2%	4.9%	6.6%	46.38	-8.0%	-1.4%	23.7%	4.1%	38.47
13-Aug	-2.1%	-0.4%	20.4%	5.5%	45.18	-4.7%	15.7%	-7.7%	8.2%	48.84	-1.4%	9.0%	4.3%	6.5%	45.19	-5.8%	-1.0%	20.3%	4.3%	37.26
14-Aug	-3.7%	-0.3%	19.2%	5.6%	43.99	-3.6%	16.1%	-10.3%	8.4%	47.66	-1.8%	8.8%	3.9%	6.4%	43.99	-3.9%	-0.6%	16.7%	4.5%	36.06
14-Aug	-2.3%	-0.3%	18.8%	5.3%	42.51	-2.6%	14.1%	-8.4%	8.2%	46.89	-2.3%	8.6%	3.2%	6.3%	42.51	-1.8%	-0.1%	12.1%	4.9%	34.58
14-Aug	-2.6%	-0.6%	17.1%	5.4%	40.97	-9.4%	12.9%	-4.6%	7.9%	45.83	-0.1%	8.9%	1.1%	6.2%	40.97	0.4%	0.0%	13.0%	4.2%	33.03
Max Ru	29.6%	-	-	-	-	-	-	-	-	-	-	-	-	26.50%	-	-	-	-	27.00%	

Table 4

Downstream flow results among the four solutions in a rolling horizon simulation.

Date	Solution D				Solution I				Solution II				Solution E			
	F ₁	F ₂	F ₃	Sum	F ₁	F ₂	F ₃	Sum	F ₁	F ₂	F ₃	Sum	F ₁	F ₂	F ₃	Sum
10-Aug	19.1%	0.0%	16.9%	35.9%	18.9%	0.0%	16.8%	35.7%	18.9%	0.0%	16.8%	35.6%	25.8%	1.4%	20.0%	47.2%
10-Aug	7.4%	0.9%	7.0%	15.4%	7.4%	0.1%	6.8%	14.3%	8.3%	0.2%	7.2%	15.6%	4.3%	5.5%	7.1%	16.9%
10-Aug	7.3%	3.1%	6.0%	16.4%	6.9%	0.1%	4.9%	11.9%	9.2%	0.6%	6.1%	15.9%	6.8%	3.9%	6.1%	16.8%
11-Aug	4.9%	4.4%	4.7%	14.1%	5.2%	2.4%	4.2%	11.9%	6.5%	2.0%	4.6%	13.1%	5.7%	3.6%	4.8%	14.1%
11-Aug	2.4%	6.4%	3.9%	12.6%	4.2%	3.8%	3.9%	11.9%	3.5%	4.7%	3.9%	12.1%	4.1%	4.2%	4.0%	12.3%
11-Aug	3.7%	4.5%	3.8%	12.0%	4.3%	3.7%	3.8%	11.7%	5.1%	2.6%	3.8%	11.4%	3.5%	4.8%	3.8%	12.0%
11-Aug	2.3%	6.7%	3.9%	12.9%	3.3%	5.1%	3.8%	12.1%	3.4%	5.0%	3.8%	12.3%	0.9%	9.3%	4.1%	14.2%
12-Aug	4.5%	3.4%	3.7%	11.6%	5.1%	2.6%	3.7%	11.4%	3.2%	5.2%	3.7%	12.2%	6.1%	1.3%	3.7%	11.0%
12-Aug	2.6%	6.1%	3.7%	12.4%	5.1%	2.5%	3.7%	11.4%	3.5%	4.8%	3.7%	12.1%	2.1%	7.7%	4.0%	13.8%
12-Aug	3.2%	5.2%	3.7%	12.0%	4.7%	3.1%	3.7%	11.5%	3.7%	4.6%	3.7%	11.9%	2.4%	7.4%	4.0%	13.8%
12-Aug	4.8%	3.0%	3.7%	11.4%	4.6%	3.3%	3.7%	11.5%	3.4%	4.9%	3.7%	12.0%	3.0%	5.6%	3.7%	12.4%
13-Aug	4.4%	3.5%	3.6%	11.6%	5.5%	2.0%	3.6%	11.1%	3.2%	5.1%	3.6%	12.0%	1.7%	7.4%	3.7%	12.8%
13-Aug	2.5%	6.1%	3.7%	12.3%	5.5%	2.0%	3.7%	11.2%	3.4%	4.9%	3.7%	12.0%	3.3%	5.0%	3.7%	12.0%
13-Aug	3.6%	4.7%	3.6%	11.8%	4.9%	2.8%	3.6%	11.3%	3.5%	4.8%	3.6%	11.9%	5.3%	2.3%	3.6%	11.2%
13-Aug	4.4%	3.5%	3.6%	11.5%	4.8%	3.0%	3.6%	11.4%	3.4%	4.9%	3.6%	11.9%	5.8%	1.7%	3.6%	11.0%
14-Aug	2.2%	6.5%	3.5%	12.3%	2.3%	5.1%	3.2%	10.5%	3.7%	4.5%	3.6%	11.8%	6.6%	0.4%	3.5%	10.6%
14-Aug	5.2%	2.5%	3.5%	11.2%	1.9%	6.0%	3.3%	11.3%	3.6%	4.6%	3.5%	11.8%	0.0%	9.6%	3.5%	13.1%
Max Rd	19.1%	6.7%	16.9%	35.9%	18.9%	6.0%	16.8%	35.7%	18.9%	5.2%	16.8%	35.6%	25.8%	9.6%	20.0%	47.2%

Table 5

Statistics of flood water conservation during historical receding floods.

Floods no.	Solution D (Million m ³)	Solution SI (Million m ³)	Solution E (Million m ³)
20,150,724	13.02	13.67 (5%)	8.61 (-33.9%)
20,160,702	69.53	82.40 (18.5%)	39.70 (-42.9%)
20,140,705	22.44	23.41 (4.3%)	14.90 (-33.6%)
20,140,713	17.14	17.19 (0.3%)	15.62 (-8.9%)
20,140,725	17.80	17.91 (0.6%)	14.96 (-16%)
20,140,813	20.08	20.38 (1.5%)	18.66 (-7.1%)
Average	26.66	29.16 (9.3%)	18.74 (-29.7%)

scenarios of future streamflow from ensemble streamflow forecasting models when cascading uncertainties can be accurately represented within a coupled error analysis models. With the advancement of ensemble flood forecasts techniques, this could be further extended in future studies.

CRediT authorship contribution statement

Bin Xu: Methodology, Software, Writing - original draft. **Ping-an Zhong:** Supervision, Conceptualization. **Qingwen Lu:** Formal analysis. **Feilin Zhu:** Validation. **Xin Huang:** Investigation. **Yufei Ma:** Data curation. **Jisi Fu:** Visualization.

Declaration of Competing Interest

The authors declare that they have no known competing financial interests or personal relationships that could have appeared to influence the work reported in this paper.

Acknowledgements

We would like to thank the anonymous reviewers for their in-depth reviews and constructive suggestions. The remarks and summary of reviewer comments provided by the Editor and Associate Editor are also greatly appreciated, which have facilitated major improvements in this paper. This study is supported by National Key Technologies R&D Program of China (Grant No. 2017YFC0405604), the Fundamental Research Funds for the Central Universities (Grant No. B200202028, B200202032), the China Postdoctoral Science Foundation Funded Project (Grant No. 2018T110525), and Qing Lan Project of Jiangsu Province. Data will be made available on contacting the first author.

Appendix A. Supplementary data

Supplementary data to this article can be found online at <https://doi.org/10.1016/j.jhydrol.2020.125513>.

References

- Cai, X., Wallington, K., Shafee-Jood, M., Marston, L., 2018b. Understanding and managing the food-energy-water nexus – opportunities for water resources research. *Adv. Water Resour.* 111, 259–273. <https://doi.org/10.1016/j.advwatres.2017.11.014>.
- Cai, C., Wang, J., Li, Z., 2018a. Improving TIGGE precipitation forecasts using an SVR ensemble approach in the Huaihe River Basin. *Adv. Meteorol.* 2018, 1–15. <https://doi.org/10.1155/2018/7809302>.
- Chen, J., Guo, S., Li, Y., Liu, P., Zhou, Y., 2013. Joint operation and dynamic control of flood limiting water levels for cascade reservoirs. *Water Resour. Manage.* 27 (3), 749–763. <https://doi.org/10.1007/s11269-012-0213-z>.
- Chen, J., Shi, H., Sivakumar, B., Peart, M.R., 2016a. Population, water, food, energy and dams. *Renewable Sustainable Energy Rev.* 56, 18–28. <https://doi.org/10.1016/j.rser.2015.11.043>.
- Chen, L., Singh, V.P., Lu, W., Zhang, J., Zhou, J., Guo, S., 2016b. Streamflow forecast uncertainty evolution and its effect on real-time reservoir operation. *J. Hydrol.* 540, 712–726. <https://doi.org/10.1016/j.jhydrol.2016.06.015>.
- Chen, L., Huang, K., Zhou, J., Duan, H., Zhang, J., Wang, D., Qiu, H., 2020. Multiple-risk assessment of water supply, hydropower and environment nexus in the water resources system. *J. Clean. Prod.* 22057. <https://doi.org/10.1016/j.jclepro.2020.122057>.
- Chen, J., Zhong, P., Zhang, Y., Navar, D., Yeh, W.W.G., 2017. A decomposition-integration risk analysis method for real-time operation of a complex flood control system. *Water Resour. Res.* 53 (3), 2490–2506. <https://doi.org/10.1002/2016WR019842>.
- Croke, H.L., Pappenberger, F., 2009. Ensemble flood forecasting: a review. *J. Hydrol.* 375 (3–4), 613–626. <https://doi.org/10.1016/j.jhydrol.2009.06.005>.
- Ding, W., Zhang, C., Peng, Y., Zeng, R., Zhou, H., Cai, X., 2015. An analytical framework for flood water conservation considering forecast uncertainty and acceptable risk. *Water Resour. Res.* 51 (6), 4702–4726. <https://doi.org/10.1002/2015WR017127>.
- Emmerich, M.T.M., Deutz, A.H., 2018. A tutorial on multiobjective optimization: fundamental and evolutionary methods. *Nat. Comput.* 17 (3), 585–609. <https://doi.org/10.1007/s11047-018-9685-y>.
- Etkin, D., Kirshen, P., Watkins, D., Roncoli, C., Sanon, M., Some, L., Dembele, Y., Sanfo, J., Zoungrana, J., Hoogenboom, G., Watkins, D., 2015. Stochastic programming for improved multiuse reservoir operation in Burkina Faso, West Africa. *J. Water Res. Plan. Man.* 141 (3), 4014056.
- Feng, Z., Niu, W., Cheng, C., 2019. China's large-scale hydropower system: operation characteristics, modeling challenge and dimensionality reduction possibilities. *Renewable Energy* 136, 805–818. <https://doi.org/10.1016/j.renene.2019.01.059>.
- Haguma, D., Leconte, R., Cote, P., 2018. Evaluating transition probabilities for a stochastic dynamic programming model used in water system optimization. *J. Water Res. Plan. Man.* 144 (040170902). [https://doi.org/10.1061/\(ASCE\)WR.1943-5452.0000883](https://doi.org/10.1061/(ASCE)WR.1943-5452.0000883).
- Haimes, Y.Y., 1977. *Hierarchical Analysis of Water Resources Systems*. Me Graw-Hill Book Co.
- Housh, M., Ostfeld, A., Shamir, U., 2013. Limited multi-stage stochastic programming for managing water supply systems. *Environ. Model. Software* 41, 53–64. <https://doi.org/10.1016/j.envsoft.2012.11.006>.
- Huang, L., Li, X., Fang, H., Yin, D., Si, Y., Wei, J., Liu, J., Hu, X., Zhang, L., 2019. Balancing social, economic and ecological benefits of reservoir operation during the

- flood season: a case study of the Three Gorges Project, China. *J. Hydrol.* 572, 422–434. <https://doi.org/10.1016/j.jhydrol.2019.03.009>.
- Huang, K., Ye, L., Chen, L., Wang, Q., Dai, L., Zhou, J., Singh, V.P., Huang, M., Zhang, J., 2018. Risk analysis of flood control reservoir operation considering multiple uncertainties. *J. Hydrol.* 565, 672–684. <https://doi.org/10.1016/j.jhydrol.2018.08.040>.
- King, A.J., Wallace, S.W., 2012. *Modeling with stochastic programming*. Springer Science & Business Media, New York.
- Kodikara, P.N., Perera, B.J.C., Kularathna, M.D.U.P., 2010. Stakeholder preference elicitation and modelling in multi-criteria decision analysis – a case study on urban water supply. *Eur. J. Oper. Res.* 206 (1), 209–220. <https://doi.org/10.1016/j.ejor.2010.02.016>.
- Labadie, J.W., 2004. Optimal operation of multireservoir systems: state-of-the-art review. *J. Water Res. Plan. Man.* 130 (2), 93–111.
- Lasdon, L.S., Fox, R.L., Ratner, M.W., 1974. Nonlinear optimization using the generalized reduced gradient method. *Recherche Opérationnelle* 8 (3), 73–103.
- Li, X., Guo, S., Liu, P., Chen, G., 2010. Dynamic control of flood limited water level for reservoir operation by considering inflow uncertainty. *J. Hydrol.* 391 (1–2), 126–134. <https://doi.org/10.1016/j.jhydrol.2010.07.011>.
- Liu, P., Li, L., Guo, S., Xiong, L., Zhang, W., Zhang, J., Xu, C., 2015. Optimal design of seasonal flood limited water levels and its application for the three gorges reservoir. *J. Hydrol.* 527, 1045–1053. <https://doi.org/10.1016/j.jhydrol.2015.05.055>.
- Mao, J., Tian, M., Hu, T., Ji, K., Dai, L., Dai, H., 2019. Shuffled complex evolution coupled with stochastic ranking for reservoir scheduling problems. *Water Sci. Eng.* 12 (4), 307–318.
- Nayak, M.A., Herman, J.D., Steinschneider, S., 2018. Balancing flood risk and water supply in California: Policy search integrating short-term forecast ensembles with conjunctive use. *Water Resour. Res.* 54 (10), 7557–7576. <https://doi.org/10.1029/2018WR023177>.
- Nester, T., Komma, J., Viglione, A., Bloeschl, G., 2012. Flood forecast errors and ensemble spread—a case study. *Water Resour. Res.* 48 (W10502). <https://doi.org/10.1029/2011WR011649>.
- Ouyang, S., Zhou, J., Li, C., Liao, X., Wang, H., 2015. Optimal design for flood limit water level of cascade reservoirs. *Water Resour. Manage.* 29 (2), 445–457. <https://doi.org/10.1007/s11269-014-0879-5>.
- Pan, L., Housh, M., Liu, P., Cai, X., Chen, X., 2015. Robust stochastic optimization for reservoir operation. *Water Resour. Res.* 51 (1), 409–429. <https://doi.org/10.1002/2014WR015380>.
- Papaefthymiou, G., Pinson, P., 2008. In: *Modeling of Spatial Dependence in Wind Power Forecast Uncertainty*. University of Puerto Rico, Mayaguez, pp. 1–9.
- Peng, Y., Chen, K., Yan, H., Yu, X., 2017. Improving flood-risk analysis for confluence flooding control downstream using copula Monte carlo method. *J. Hydrol. Eng.* 22 (040170188). [https://doi.org/10.1061/\(ASCE\)HE.1943-5584.0001526](https://doi.org/10.1061/(ASCE)HE.1943-5584.0001526).
- Piantadosi, J., Metcalfe, A.V., Howlett, P.G., 2008. Stochastic dynamic programming (SDP) with a conditional value-at-risk (CVaR) criterion for management of stormwater. *J. Hydrol.* 348 (3–4), 320–329. <https://doi.org/10.1016/j.jhydrol.2007.10.007>.
- Piao, S., Ciais, P., Huang, Y., Shen, Z., Peng, S., Li, J., Zhou, L., Liu, H., Ma, Y., Ding, Y., Friedlingstein, P., Liu, C., Tan, K., Yu, Y., Zhang, T., Fang, J., 2010. The impacts of climate change on water resources and agriculture in China. *Nature* 467 (7311), 43–51. <https://doi.org/10.1038/nature09364>.
- Sahukhal, R., Bajracharya, T.R., 2019. Modeling water resources under competing demands for sustainable development: a case study of Kaligandaki Gorge Hydropower Project in Nepal. *Water Sci. Eng.* 12 (1), 19–26. <https://doi.org/10.1016/j.wse.2019.03.002>.
- Shi, H., Chen, J., Wang, K., Niu, J., 2018. A new method and a new index for identifying socioeconomic drought events under climate change: a case study of the East River basin in China. *Sci. Total Environ.* 616–617, 363–375. <https://doi.org/10.1016/j.scitotenv.2017.10.321>.
- Si, W., Gupta, H.V., Bao, W., Jiang, P., Wang, W., 2019. Improved dynamic system response curve method for real-time flood forecast updating. *Water Resour. Res.* 55 (9), 7493–7519. <https://doi.org/10.1029/2019WR025520>.
- Sklar, A., 1959. Fonctions de répartition à dimensions et leurs marges. *Sci. Res.* 8.
- Tan, Q., Wang, X., Liu, P., Lei, X., Cai, S., Wang, H., Ji, Y., 2017. The dynamic control bound of flood limited water level considering capacity compensation regulation and flood spatial pattern uncertainty. *Water Resour. Manage.* 31 (1), 143–158. <https://doi.org/10.1007/s11269-016-1515-3>.
- Tang, R., Ding, W., Ye, L., Wang, Y., Zhou, H., 2019. Tradeoff analysis index for many-objective reservoir optimization. *Water Resour. Manage.* 33 (13), 4637–4651. <https://doi.org/10.1007/s11269-019-02363-z>.
- Tsoukalas, I., Makropoulos, C., 2015. Multiobjective optimisation on a budget: exploring surrogate modelling for robust multi-reservoir rules generation under hydrological uncertainty. *Environ. Modell. Software* 69, 396–413. <https://doi.org/10.1016/j.envsoft.2014.09.023>.
- Turgeon, A., 2007. Stochastic optimization of multireservoir operation: the optimal reservoir trajectory approach. *Water Resour. Res.* 43 (5). <https://doi.org/10.1029/2005WR004619>.
- Wan, W., Zhao, J., Lund, J.R., Zhao, T., Lei, X., Wang, H., 2016. Optimal hedging rule for reservoir refill. *J. Water Res. Plan. Man.* 142 (11).
- Watkins, D., McKinney, D., 1997. Finding robust solutions to water resources problems. *J. Water Resour. Plann. Manage.* ASCE 123 (1), 49–58.
- Wen, X., Liu, Z., Lei, X., Lin, R., Fang, G., Tan, Q., Wang, C., Tian, Y., Quan, J., 2018. Future changes in Yuan River ecohydrology: Individual and cumulative impacts of climates change and cascade hydropower development on runoff and aquatic habitat quality. *Sci. Total Environ.* 633, 1403–1417. <https://doi.org/10.1016/j.scitotenv.2018.03.309>.
- Wu, Y., Zhong, P., Xu, B., Zhu, F., Ma, B., 2017. Changing of flood risk due to climate and development in Huaihe River basin, China. *Stoch. Environ. Res. Risk A* 31 (4), 935–948. <https://doi.org/10.1007/s00477-016-1262-2>.
- Xu, B., Zhong, P., Zambon, R.C., Zhao, Y., Yeh, W.W.G., 2015. Scenario tree reduction in stochastic programming with recourse for hydropower operations. *Water Resour. Res.* 51 (8), 6359–6380. <https://doi.org/10.1002/2014WR016828>.
- Xu, B., Boyce, S.E., Zhang, Y., Liu, Q., Guo, L., Zhong, P., 2017. Stochastic programming with a joint chance constraint model for reservoir refill operation considering flood risk. *J. Water Res. Plan. Man.* 143 (1), 4016067. [https://doi.org/10.1061/\(ASCE\)WR.1943-5452.0000715](https://doi.org/10.1061/(ASCE)WR.1943-5452.0000715).
- Xu, B., Zhu, F., Zhong, P., Chen, J., Liu, W., Ma, Y., Guo, L., Deng, X., 2019. Identifying long-term effects of using hydropower to complement wind power uncertainty through stochastic programming. *Appl. Energy* 253, 113535. <https://doi.org/10.1016/j.apenergy.2019.113535>.
- Xu, B., Huang, X., Zhong, P., Wu, Y., 2020. Two-phase risk hedging rules for informing conservation of flood resources in reservoir operation considering inflow forecast uncertainty. *Water Resour. Manage.* <https://doi.org/10.1007/s11269-020-02571-y>.
- Yeh, W.W., 1985. Reservoir management and operations models: a state-of-the-art review. *Water Resour. Res.* 21 (12), 1797–1818. <https://doi.org/10.1029/WR021i012p01797>.
- Yun, R., Singh, V.P., 2008. Multiple duration limited water level and dynamic limited water level for flood control, with implications on water supply. *J. Hydrol.* 354 (1–4), 160–170. <https://doi.org/10.1016/j.jhydrol.2008.03.003>.
- Zhang, C., Chen, X., Li, Y., Ding, W., Fu, G., 2018. Water-energy-food nexus: concepts, questions and methodologies. *J. Clean. Prod.* 195, 625–639. <https://doi.org/10.1016/j.jclepro.2018.05.194>.
- Zhang, X., Liu, P., Xu, C., Gong, Y., Cheng, L., He, S., 2019. Real-time reservoir flood control operation for cascade reservoirs using a two-stage flood risk analysis method. *J. Hydrol.* 577, 123954. <https://doi.org/10.1016/j.jhydrol.2019.123954>.
- Zhao, R., 1992. The Xinanjiang model applied in China. *J. Hydrol.* 135 (1), 371–381. [https://doi.org/10.1016/0022-1694\(92\)90096-E](https://doi.org/10.1016/0022-1694(92)90096-E).
- Zhao, T.T.G., Yang, D.W., Cai, X.M., Zhao, J.S., Wang, H., 2012. Identifying effective forecast horizon for real-time reservoir operation under a limited inflow forecast. *Water Resour. Res.* 48 (W01540). <https://doi.org/10.1029/2011WR010623>.
- Zhao, T., Zhao, J., Yang, D., Wang, H., 2013. Generalized martingale model of the uncertainty evolution of streamflow forecasts. *Adv. Water Resour.* 57, 41–51. <https://doi.org/10.1016/j.advwatres.2013.03.008>.
- Zhong, P., Kong, Y., Wang, X., Xu, B., Wang, Y., 2014. Study on method for estimation of dynamic control bounds of flood limited water level in cascade reservoirs. *J. Hydroelectr. Eng.* 33 (5), 36–43.
- Zhou, Y., Guo, S., Liu, P., Xu, C., 2014. Joint operation and dynamic control of flood limiting water levels for mixed cascade reservoir systems. *J. Hydrol.* 519, 248–257. <https://doi.org/10.1016/j.jhydrol.2014.07.029>.
- Zhou, Y., Guo, S., Chang, F., Liu, P., Chen, A.B., 2018. Methodology that improves water utilization and hydropower generation without increasing flood risk in mega cascade reservoirs. *Energy* 143, 785–796. <https://doi.org/10.1016/j.energy.2017.11.035>.
- Zhu, F., Zhong, P., Sun, Y., 2018. Multi-criteria group decision making under uncertainty: application in reservoir flood control operation. *Environ. Modell. Software* 100, 236–251. <https://doi.org/10.1016/j.envsoft.2017.11.032>.